MONTANA STATE UNIVERSITY

Natural convection heat transfer within enclosures at reduced pressures
by Peter Kevin Brown

A thesis submitted in partial fulfillment of the requirements for the degree of MASTER OF SCIENCE in Mechanical Engineering
Montana State University
© Copyright by Peter Kevin Brown (1980)

Abstract:
Natural convection heat transfer in air within enclosures has been investigated over the pressure range of 2670-86,180 Pa (20-646.4 mm Hg), Dimensionless correlations have been generated from the data; The best correlation found included a correction for the air density: Nul = .342 RaL^1/4 (ρ/ρatn,)^.129 where L is the hypothetical gap width. The Rayleigh number in the experiments ranged over 1x10^3 - 2x10^6. The geometries used were cylinder-cube (inner body-outer body) and cube-cube, with the bodies mounted concentrically in both cases. Temperature profiles at four positions (0°, 34°, 80°, and 160° from the upward vertical) were measured for the cylinder-cube case. The thickening of the boundary layer at low pressures and the region of constant temperature between the bodies at high Ra were clearly observed.

STATEMENT OF PERMISSION TO COPY

In presenting this thesis in partial fulfillment of the requirements for an advanced degree at Montana State University, I agree that the Library shall make it freely available for inspection. I further agree that permission for extensive copying of this thesis for scholarly purposes may be granted by my major professor, or, in his absence, by the Director of Libraries. It is understood that any copying or publication of this thesis for financial gain shall not be allowed without my written permission.

Signature Peter K. Brown

Date 16 September 1980

NATURAL CONVECTION HEAT TRANSFER WITHIN ENCLOSURES AT REDUCED PRESSURES

by

PETER KEVIN BROWN

A thesis submitted in partial fulfillment
of the requirements for the degree

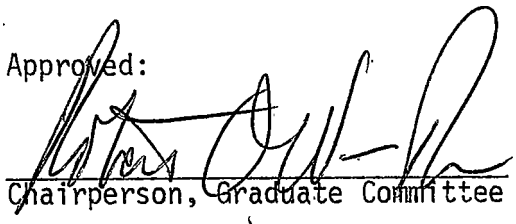
of

MASTER OF SCIENCE

in

Mechanical Engineering

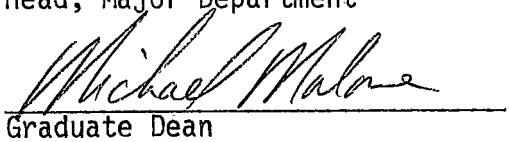
Approved:



Chairperson, Graduate Committee



Head, Major Department



Graduate Dean

MONTANA STATE UNIVERSITY
Bozeman, Montana

September, 1980

ACKNOWLEDGEMENTS

The author wishes to thank Dr. R. L. Mussulman for reading the original typescript and especially Dr. R. O. Warrington for guidance and suggestions throughout the completion of this work. Sincere thanks are also due to Charlene Townes for typing the final copy of the thesis.

TABLE OF CONTENTS

Chapter	Page
VITA	ii
ACKNOWLEDGEMENT	iii
LIST OF TABLES	v
LIST OF FIGURES	vi
NOMENCLATURE	vii
ABSTRACT	x
I. INTRODUCTION	1
II. LITERATURE REVIEW	3
III. EXPERIMENTAL APPARATUS AND PROCEDURE	13
IV. HEAT TRANSFER AND TEMPERATURE PROFILE RESULTS	21
V. A MODIFICATION OF THE METHOD OF RAITHBY AND HOLLANDS FOR CUBICAL GEOMETRIES	57
VI. CONCLUSIONS	75
APPENDIX I. DERIVATION OF THE METHOD OF RAITHBY AND HOLLANDS	77
APPENDIX II. DATA REDUCTION PROGRAMS	86
APPENDIX III. PARTIALLY REDUCED DATA	96
BIBLIOGRAPHY	102

LIST OF TABLES

Table		Page
4.1	Range of Geometries and Correlating Parameter	22
4.2	Correlation Equations for All Data	27
4.3	Fit of Present Data to Previous Correlations	35
4.4	Correlation Equations from the Variable Density Data Alone	36
4.5	Density-Corrected Correlations for the Variable Density Data	45
4.6	Density-Corrected Correlations for All Data	47
5.1	Correlations (5.8) and (5.9) with the Variable Density Data	62
5.2	Correlations (5.8) and (5.9) with All Data	63

LIST OF FIGURES

Figure		Page
3.1	Schematic of Heat Transfer Apparatus with Supporting Instrumentation	14
4.1	Local Gap Width a for the Cylinder-Cube Geometry	25
4.2	All of the Heat Transfer Data: Nu_L vs. Ra_L	26
4.3	All of the Heat Transfer Data: Nu_b vs. Ra_b	30
4.4	All of the Heat Transfer Data: Q vs. Ra_L	32
4.5	Variable-Density Data, Cylinder-Cube Geometry	39
4.6	Variable-Density Data, Cube-Cube Geometry	40
4.7	All of the Variable-Density Data: $Nu_{L''}$ vs. $Ra_{L''}$	43
4.8	Temperature Profile Data at Two Different Pressures: Solid Lines--ΔT=23.3°C (42.0°F), Pressure=16.3 mm Hg; Open Symbols--ΔT=20.7°C (37.2°F), Pressure=641.9 mm Hg	50
4.9	Temperature Profiles at Two Different Pressures: Solid Lines--ΔT=30.2°C (54.5°F), Pressure=48.0 mm Hg; Open Symbols--ΔT=18.7°C (33.6°F), Pressure=149.6 mm Hg	51
4.10	Temperature Profile Data at Two Different Pressures: Solid Lines--ΔT=23.8°C (42.8°F), Pressure=248.8 mm Hg; Open Symbols--ΔT=22.9°C (41.3°F), Pressure=505.7 mm Hg	52
4.11	Temperature Profile Data: ΔT=22.8°C (41.1°F), Pressure=396.8 mm Hg	53
5.1	Nomenclature for the Cylinder-Cube Geometry	59
5.2	Nomenclature for Flow Around a Cube	65
5.3	Idealization of Flow Around a Cube: The Shaded Regions are of Equal Area	66
A1.1	Nomenclature of the Method of Raithby and Hollands	79
A1.2	Nomenclature for Two-Dimensional or Axisymmetric Flow	84

NOMENCLATURE

Symbol	Description
a	Any characteristic length
b	Boundary layer length on the inner body
C, C_{1-4}	Empirically determined constants
c_p	Constant pressure heat capacity
d	Length of a side of a cube
$D_i (D_o)$	Diameter of a sphere of surface area equal to that of the inner (outer) body
g	Acceleration due to gravity
g_x	Gravitational acceleration in the direction of the x coordinate
Gr	The Grashof number, $g\beta(T_i-T_o)a^3\rho^2/\mu^2$
$\bar{h}$	Average heat transfer coefficient, $q''/(T_i-T_o)$
k	Thermal conductivity of air
L, L', L"	Gap widths as defined on p. 23-24
$\mathring{m}_i$ ($\mathring{m}_o$)	Mass flow rate in the inner (outer) region of the boundary layer
mm Hg	A unit of pressure, 760 mm Hg = 1 atmosphere
M	$(T_m-T_s)/(T_\infty-T_s)$
Nu	The Nusselt number, $\bar{h}a/k$
P	Pressure of air at experimental conditions
Pa	A unit of pressure, 101,325 Pa = 1 atmosphere
Pr	The Prandtl number, $\mu c_p/k$

Symbol	Description
q or q_{conv}	Heat transferred by natural convection
q_{cond}	Heat transferred by conduction through a stagnant fluid under similar conditions
q''	Heat transferred by convection per unit area
Q	q_{conv}/q_{cond}
r	Radius of curvature
r^*	Dimensionless radius defined on p.19
R_i (R_o)	Radius of a sphere of volume equal to that of the inner (outer) body
Ra	The Rayleigh number, Gr·Pr
S	Length of the x coordinate along a body
T	Temperature
T_i (T_o)	Inner (outer) body temperature
T_s	Temperature at the wall
T_∞	Temperature far away from the wall
T^*	Dimensionless temperature defined on p.19
T_m	Temperature at y_m or temperature in the fluid between the inner and outer equivalent conduction layers
$\overline{T}_i$ ($\overline{T}_o$)	Average temperature in the inner (outer) region of the boundary layer
$\overline{T}_m$	Average temperature between the inner and outer equivalent conduction layers
ΔT_r	A reference temperature difference
u	Velocity component in the direction of x
u_{max}	Maximum velocity in the profile

Symbol	Description
x	Coordinate along the body in the direction of flow
y	Coordinate out of the body normal to x
y_m	Location of the velocity maximum in the profile
β	Thermal expansivity of air $(1/V)(dV/dT)$, where V is the volume; for an ideal gas $\beta = 1/T$
Γ_i (Γ_o)	Mass flow rate per unit depth in the inner (outer) region of the boundary layer
δ	Boundary layer thickness or any one of three gap widths L, L', or L"
$\Delta(x)$ or $\Delta_\ell(x)$	Local equivalent conduction layer thickness
$\overline{\Delta}$ or $\overline{\Delta}_\ell$	Average equivalent conduction layer thickness
η	Dimensionless y coordinate, y/δ
μ	Viscosity of air
ρ	Density of air in the experimental conditions
ρ_{atm}	Density of air at atmospheric pressure and standard temperature (298.15°K)

ABSTRACT

Natural convection heat transfer in air within enclosures has been investigated over the pressure range of 2670-86,180 Pa (20-646.4 mm Hg). Dimensionless correlations have been generated from the data. The best correlation found included a correction for the air density:

$$Nu_L = .342\ Ra_L^{1/4}\ (\rho/\rho_{atm})^{.129}$$

where L is the hypothetical gap width. The Rayleigh number in the experiments ranged over $1x10^3$ - $2x10^6$. The geometries used were cylinder-cube (inner body-outer body) and cube-cube, with the bodies mounted concentrically in both cases. Temperature profiles at four positions (0°, 34°, 80°, and 160° from the upward vertical) were measured for the cylinder-cube case. The thickening of the boundary layer at low pressures and the region of constant temperature between the bodies at high Ra were clearly observed.

CHAPTER I

INTRODUCTION

The phenomenon of natural convection heat transfer within enclosures has received a great deal of attention in recent years. There is a growing demand for an understanding of this phenomenon in such areas as nuclear design, electronic packaging, space heating, and solar collector design. The majority of this effort has been experimental. The nonlinearity and coupling of the governing differential equations of continuity, momentum, and energy have made analytical solutions difficult to find. Those few that exist apply only to relatively simple geometries, such as concentric cylinders or spheres.

In the present study, natural convection heat transfer in air from an isothermal (heated) inner body to an isothermal (cooled) outer body was investigated. More specifically, rates of heat transfer were measured for various temperature differences between the bodies and different pressures of air in the test space. The outer body was cubical; the inner bodies were a vertical cylinder with hemispherical end caps and a cube.

The primary purpose of this investigation was to find an empirical correlation for the heat transferred by natural convection in air from a body to its enclosure as a function of air pressure (i.e., vacuum). The Rayleigh number in these experiments ranged over 10^3 - 2 x 10^6. Since evacuation of the cavity surrounding a heated device, such as a solar collector tube, is an effective way to reduce heat loss [1-3], such a

relationship would be quite useful. The correlations found were tested against previous results. In addition, a correlation based on the method of Raithby and Hollands [4] was developed and tested against the data.

Temperature profiles were also measured for some of the heat transfer conditions. The profiles are useful for elucidating general trends, such as the thickening of the boundary layer at low pressure. In addition, they may provide a means of verification for any future numerical or analytical solutions which may be advanced.

CHAPTER II

LITERATURE REVIEW

Natural convection phenomena fall broadly into two categories: convection in an infinite fluid bath, or external convection, and convection within an enclosure, or internal convection. The following review is intended to provide a background for the present investigation and is not a complete survey of research in natural convection.

Dimensional analysis has shown [5,6] that external natural convection may be correlated by

$$Nu_a = f(Gr_a, Pr)$$

where a is some characteristic dimension and

$$Nu_a = \frac{\bar{h}\, a}{k} \qquad \text{(Nusselt number)},$$

$$Gr_a = \frac{g\beta\, \Delta T\, a^3\, \rho^2}{\mu^2} \qquad \text{(Grashof number)},$$

and

$$Pr = \frac{\mu c_p}{k} \qquad \text{(Prandtl number)}.$$

Often the effects of Gr_a and Pr can be combined by

$$Nu_a = f(Ra_a), \text{ where}$$

$$Ra_a = Gr_a \cdot Pr \qquad \text{(Rayleigh number)}.$$

In this investigation, Ra_a will be varied largely by variations in ρ (i.e., pressure of the air) and also by variations in a and in ΔT.

Elenbaas [7] developed some early correlations for external natural convection heat transfer from a vertical cylinder:

$$Nu_{d,w}\exp(-2/Nu_{d,w}) = 0.6Ra_{d,w}^{1/3}/Ra_{h,w}^{1/12}$$

and from a horizontal cylinder:

$$Nu_{d,w}\exp(-2/Nu_{d,w}) = 0.16Ra_{d,w}^{1/3}/g(Ra_{d,w})$$

where $g(Ra_{d,w})$ is a function presented graphically. The subscript d refers to the diameter and h to the height of the cylinder, and w means that the fluid properties are to be evaluated at the wall temperature.

King [8] correlated external natural convection from several geometric shapes, including ones similar to those used in this investigation, by

$$Nu_D = 0.60\ Ra_D^{1/4} \text{ for } 10^4 < Ra_D < 10^9$$

where $$\frac{1}{D} = \frac{1}{\text{vertical dimension}} + \frac{1}{\text{horizontal dimension}}.$$

Holman [6] reports a correlation for a vertical cylinder of

$$Nu_h = 0.59Ra_h^{1/4} \text{ for } \frac{D}{h} \geq \frac{35}{Gr_h^{1/4}}$$

where D is the diameter and h the height of the cylinder.

Lienhard [9] found that laminar external convection could be correlated well by a balance of buoyancy and viscous forces on the body.

Using velocity and temperature profiles for a flat plate, he obtained

$$Nu_b = 0.52Ra_b^{1/4}$$

where b is the length of the thermal boundary layer on the body.

There have been several experimental and analytical investigations of external convection to air at low Ra (low pressure of air, small characteristic dimension, or small ΔT). Saunders [10] performed early experiments on the pressure dependency of convection in air. He found that Nu_h for a vertical flat plate falls well above accepted correlations for $Ra_h < 10^5$. This is seen as a leveling off of Nu to near unity as a pure conduction regime is entered at low pressure. Kyte, Madden, and Piret [11] extended low pressure measurements to a vacuum in which the mean free path of the air molecules becomes comparable to the physical body dimensions. They found for vertical wires that

$$Nu_{D'} = \frac{2}{\ln[1+4.47/(Ra_{D'}\frac{D'}{h})^{0.26}]}$$

in the molecular flow regime. Here h is the height of the wire (cylinder) and D' is the diameter plus twice the mean free path of the gas.

Gryzagordis [12] reports that a vertical plate in air at low pressures obeys the standard correlation

$$Nu_h = 0.555Ra_h^{1/4}$$

down to Ra_h=10, in contrast to Saunders [10] and to Suriano and Yang [13]. The latter study suggests that the Nusselt number should fall above this correlation for Ra_h lower than about 500. The interested reader is referred to the literature for further details.

Analytical and numerical solutions of external natural convection are based on solving the coupled differential equations of continuity, momentum, and energy in the boundary layer approximation [5]. The solutions usually take the form of series solutions in Ra for the temperature and stream functions. Chiang, Ossin, and Tien [14] solved the case of an isothermal sphere and presented graphical results of velocity and temperature profiles and local Nusselt numbers. Lin and Chao [15] and Saville and Churchill [16] presented similar results for two-dimensional and axisymmetric cases. Sparrow and Gregg [17] solved the equations for a vertical cylinder and developed a condition under which it may be correlated by the flat plate result:

$$\frac{2^{1/2}}{Gr^{1/4}}(h/D) \leq 0.15.$$

Minkowycz and Sparrow [18] used the technique of local non-similarity to solve the case of a vertical cylinder. The cases solved ranged from near the flat plate solution to a factor of four deviation from it. The reader is directed to the literature for further information. Finally, Churchill and Churchill [19] have presented a correlating equation for all geometries of external natural convection, in both laminar and turbu-

lent flow:

$$Nu^{1/2}=Nu_o^{1/2} + \left\{\frac{Ra/300}{[1+(0.5/Pr)^{9/16}]^{16/9}}\right\}^{1/6}.$$

Values are tabulated for Nu_o, the Nusselt number in the limit as Ra approaches zero, and characteristic lengths are given for various geometries. In addition, corrections are outlined to account for non-Newtonian fluids and simultaneous heat and mass transfer.

The great majority of work in internal natural convection has been experimental. An early study by Elenbaas [20] with parallel vertical plates led to the following correlation:

$$Nu_D = \frac{1}{2}\frac{D}{h} Ra_D[1-\exp(-35h/DRa_D)]^{3/4}$$

where D is the plate spacing and h is the height. Holman [6], for the same geometry, gives the following correlation:

$$Nu_D = 0.197Ra_D^{1/4} (D/h)^{1/9} \quad \text{for} \quad 6x10^3 \leq Ra_D \leq 2x10^5$$

with the lengths defined as before. In an analytical study of parallel plates, Batchelor [21] recommends using

$$Nu_D = 0.48Ra_D^{1/4} (h/D)^{3/4} \quad \text{for} \quad \frac{Ra_D}{500} > \frac{h}{D}.$$

Newell and Schmidt [22] made an analytical study of long rectangular enclosures with adiabatic top and bottom surfaces and isothermal walls at

two different temperatures. The resulting correlations were

$$Nu_D = 0.0547Gr_D^{0.397} \quad , \quad \frac{h}{D} = 1$$

and $$Nu_D = 0.155Gr_D^{0.315}(h/D)^{-0.265} \quad , \quad 2.5 \leq \frac{h}{D} \leq 20 \ .$$

Randall, Mitchell, and El-Wakil [23] experimented with rectangular enclosures tilted at various angles and reported

$$Nu_D = 0.118[Ra_D \cos^2(\phi - 45°)]^{0.29} \ .$$

In these experiments, ϕ, the angle from the horizontal, varied from 45-90°, the aspect ratio h/D varied from 9-36, and Ra_D varied from $2.8x10^3$-$2.2x10^5$.

Flack, Konopnicki, and Rooke [24] performed heat transfer experiments with an isoceles triangular enclosure with an adiabatic bottom face and isothermal rising walls of different temperatures. The apex angle was varied so that the aspect ratio (height/base width) ranged from 0.29-0.87. They correlated their results by

$$Nu_l = c_3(Gr_l)^{c2} + 1.589/\cos\theta$$

where θ is the angle of the rising walls from the horizontal and l is their length. The constants are tabulated for values of θ. The trigonometric term in the correlation is to account for conduction near the apex, where the isothermal surfaces are close together.

Scanlan, Bishop, and Powe [25] measured convection between concentric spheres. They defined an effective thermal conductivity

$$\frac{k_{eff}}{k} = \frac{q(r_o-r_i)}{4\pi k\Delta T r_i r_o}$$

and recommend the following correlation:

$$\frac{k_{eff}}{k} = 0.117Ra_L^{0.276} \quad , \quad 1.4x10^4 < Ra_L < 2.5x10^6$$

where L is the gap width r_o-r_i.

Kuehn and Goldstein [26-28] have analytically and experimentally treated the case of concentric and eccentric horizontal cylinders. They present correlations based on the ratio of actual convection heat transfer to that which would be conducted through a stagnant film layer under the same conditions. For air they present

$$Q = q_{conv}/q_{cond} = 0.159Ra_L^{0.272} \quad , \quad 2.1x10^4 \leq Ra_L \leq 9.6x10^4$$

where L is the gap width. L/D_i=0.8 in these experiments. Itoh, Fujita, Nishiwaki, and Hirata [43] propose a correlation for concentric cylinders based on a different characteristic length:

$$Nu = 0.20Ra^{1/4} \quad , \quad Ra \geq 7.1x10^3$$

where

$$Nu = \frac{\bar{h}_i r_i \ln(r_o/r_i)}{k} = \frac{\bar{h}_o r_o \ln(r_o/r_i)}{k}$$

and $$Ra = \frac{g\beta\Delta T[\sqrt{r_i r_o}\ \ln(r_o/r_i)]^3\ c_p\rho^2}{k\rho}\ .$$

There exist few studies of internal natural convection in air at low pressures. Mack and Hardee [29] have examined this problem for concentric spheres, and Mack and Bishop [30] have done so for concentric cylinders. These are analytical studies in which power series solutions in Ra are developed for the temperature and stream functions. Graphical results are presented for velocity and temperature profiles and local Nusselt numbers. The reader is referred to the literature for additional information.

Koshmarov and Ivanov [31] have published an experimental investigation of natural convection between concentric cylinders at very low pressures. Over the range of $10^{-3}<Gr_L<10^4$ they correlate the convection results by

$$Q = A\left\{\frac{2}{1+T_o/T_i}\right\}^{(1-A)}$$

where $$A = \left\{1+\frac{19}{3}\frac{Kn_i}{\ln(D_o/D_i)}\right\}^{-1}\ .$$

Temperatures here are absolute. Kn_i is the Knudsen number, defined by

$$Kn_i = \frac{\text{mean free path}}{D_i}\ .$$

Recently, Marker and Leal [32] have reported an analytical result for convection in shallow vertical annuli (three-dimensional flow):

$$Nu_h = \frac{A}{\gamma \ln(\frac{1+\gamma}{\gamma})} \; 1+2.76\times10^{-6} \frac{(Ra_h A)^2}{\gamma \ln(\frac{1+\gamma}{\gamma})^2}$$

where $$A = \frac{h}{r_o - r_i} \quad \text{and} \quad \gamma = \frac{Ar_i}{h} .$$

Raithby and Hollands [4] have developed an analysis similar to, but more refined than, Lienhard's [9] boundary layer analysis. The method involves a balance of bouyancy and viscous forces very close to the wall, along with an assumed form for the temperature profile. New correlations generated by this method include

$$Q = \frac{0.317 \ln(D_o/D_i)}{L^{3/4}(D_i^{-3/5}+D_o^{-3/5})^{5/4}} Ra_L^{1/4}$$

for concentric cylinders and

$$Q = \frac{0.61 L^{1/4} Ra_L^{1/4}}{D_o D_i (D_i^{-7/5}+D_o^{-7/5})^{5/4}}$$

for concentric spheres. This method will be gone into in greater detail later (see Chapter V).

The present investigation is essentially a continuation of work by Warrington [33] with the same apparatus. His work involved a wide variety of enclosure geometries and fluids with a large range of Prandtl numbers. The best correlation overall from his data was

$$Nu_L = 0.425 Ra_L^{0.234} (L/R_i)^{0.498} .$$

For the cylinder-cube geometry (inner body-outer body) the best correlation was

$$Nu_b = 0.593Ra_b^{0.240}(L/R_i)^{0.434}$$

and for the cube-cube geometry,

$$Nu_L = 0.322Ra_L^{0.244}(L/Ri)^{0.466}Pr^{0.0185} .$$

The better correlations for air in all geometries were

$$Q = 0.468Ra_L^{0.172}\ (L/R_i)^{0.167} ,$$

$$Nu_L = 0.612Ra_L^{0.207}\ (L/R_i)^{0.508} ,$$

and

$$Nu_b = 0.570Ra_b^{0.228}\ (L/R_i)^{0.162} .$$

In these equations, L is the gap width between hypothetical concentric spheres of volumes equal to the actual volumes of the inner and outer bodies. R_i is the radius of such an inner sphere. b is the distance traveled by the thermal boundary layer on the actual inner body, assuming no flow separation. These correlations will be tried with the present data and compared to any new correlations found.

CHAPTER III

EXPERIMENTAL APPARATUS AND PROCEDURE

The apparatus used in this investigation (see Figure 3.1) was a cubical test space 26.67 cm (10.5 in) along an inner side, fabricated from 1.27 cm (0.5 in) type 6061 aluminum. A water jacket enclosure of the same material surrounded this cube; it measured 35.56 cm (14.0 in) along an inner side. The two enclosures were fastened together with machine screws and sealed with silicone rubber sealant. Access was gained into the test space by removing the water jacket lid and a 25.4 cm (10.0 in) circular cover in the top face of the test space. The water jacket lid was sealed with a gasket; the circular cover was flanged and sealed with an O-ring and high-vacuum grease. The 3.2 cm (1.25 in) channels separating the two enclosures contained cooling water. The water flow was separately adjustable along each of the six cube faces. The cooling water was collected from the test apparatus through a drain manifold and pumped through a chiller apparatus, into an insulated storage tank, and from there through the supply manifold and back into the test apparatus.

Two heated inner bodies were used in this investigation: a cylinder with hemispherical end caps, 11.43 cm (4.5 in) in diameter and 22.61 cm (8.9 in) in overall length; and a cube measuring 12.70 cm (5.0 in) along a side. The inner bodies were each mounted on a 1.27 cm (0.5 in) stainless steel stem of .159 cm (.0625 in) wall thickness. The leads to the thermocouples and heater tapes on the inner body passed through this

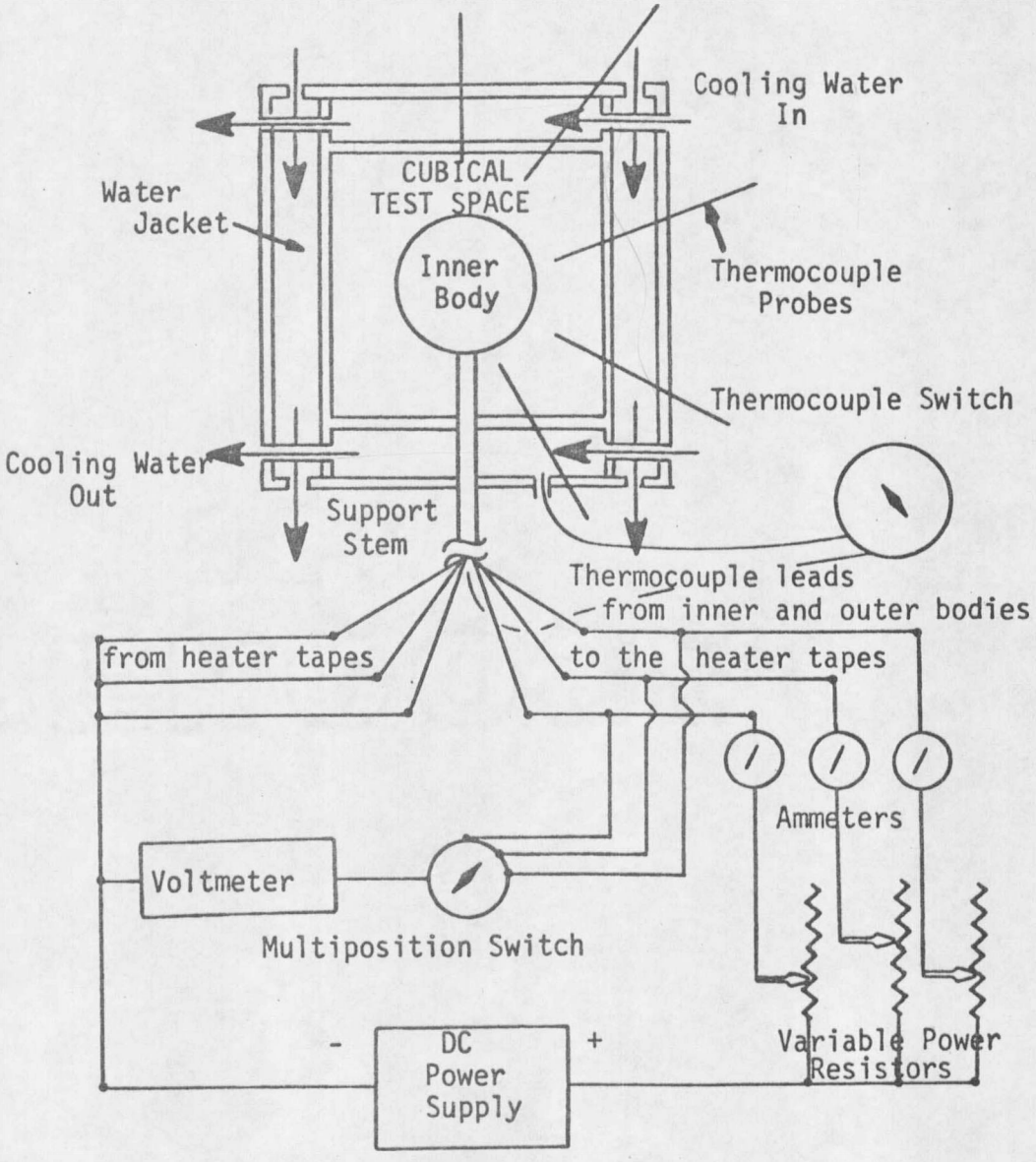


Figure 3.1 Schematic of Heat Transfer Apparatus With Supporting Instrumentation

stem. The stem in turn passed through centrally located holes of 1.27 cm (0.5 in) diameter in the bottom faces of the test space and water jacket enclosures. The holes were grooved and fitted with O-rings to seal against the stem. The stems were insulated with heat-shrinkable tubing to minimize convection heat loss to the working fluid. Flow visualization pictures taken in a similar apparatus (but with a transparent face into the test space) have clearly shown this to be effective [33]. The stem passed through a 1.27 cm (0.5 in) Conax compression fitting beneath the water jacket enclosure. This fitting eliminated leakage of air between the shrink tubing and the stem and allowed the inner body to be positioned vertically within the system.

Heat was supplied to the surface of the inner bodies by a series of heater tapes of .51 cm (.2 in) thickness, .32 cm (.126 in) width, and 28.87 ohms/m (8.8 ohms/ft) resistance per unit length. Input voltages to the tapes were individually variable by means of Ohmite rheostats (0-35 ohms, 150 watts, 2.07 amperes maximum) connected in series with the tapes. The inner bodies were constructed of sheet copper, of either .064 cm (.025 in) (cylinder) or .318 cm (.125 in) (cube) thickness. Insulating material was packed inside the inner bodies to cut down on convection within them. There were thus three factors which contributed to maintaining an isothermal heated surface on the inner bodies: 1. Individually controllable heater tapes attached to separate areas of the surfaces; 2. Low convective activity within the bodies; and 3. Fabrica-

tion from a high thermal conductivity material which promotes a "conduction smearing" effect.

Temperatures were monitored in these experiments by means of copper-constantan thermocouples and a United Systems Corp.-Digitec 268 digital millivoltmeter. There were 25 thermocouples epoxied .318 cm (.125 in) from the inner surface of the cubical test space enclosure. The number of thermocouples per face of the cube varied from 3 to 7. All thermocouples on a given face were connected in parallel, since it has been found that the temperature across any face varied no more than .8°C (1.5°F) [33].

Thermocouples were mounted flush on the inner surface of the cylindrical inner body and .165 cm (.065 in) beneath the outer surface of the cubical inner body. All thermocouples were flattened for about 2.5 cm (1 in) along the inner bodies and the outer body to minimize conduction heat transfer along the leads and resultant error in temperature measurement. Thermocouples were positioned on the inner body so that at least one thermocouple lay within each heater tape winding.

Temperature profiles between the inner and outer bodies were measured with thermocouples epoxied in the ends of .16 cm (.0625 in) o.d. stainless steel tubes. Four such temperature probes were used in this investigation, positioned at 0°, 34°, 80°, and 160° from the upward vertical. The 80° probe was mounted in a vertical plane passing diagonally through the center of the cube; the other three probes were in a

vertical plane through the center and perpendicular to two opposite vertical faces. The stainless steel probes were positioned within probe holders, each of which consisted of a .95 cm (.375 in) o.d. stainless steel tube with a .159 cm (.0625 in) i.d. Conax compression fitting welded on the outer end and .95 cm (.375 in) SAE threads cut in the inner end. The probe passed through a .18 cm (.07 in) hole in the inner end of the probe holder, and was sealed and held in place by the Conax fitting. The cubical test space enclosure had holes drilled and threaded to accept the probe holes. These holes were seated and sealed against the holders with O-rings approximately .25 cm (.1 in) from the inner surface of the cube. The probes passed through .19 cm (.075 in) holes in these seats and thus into the test space. The probe holders passed through 1.02 cm (.4 in) holes in the water jacket enclosure and were sealed there with O-rings.

To perform experiments, the inner body was positioned within the test space, the thermocouple leads were connected to the millivoltmeter along with a standard reference at 0°C (32°F), and the heater tape leads were connected to the power supply. The circular cover and water jacket lid were attached and sealed, and all temperature probes were positioned within their holders. The test space was evacuated to the desired vacuum by means of a Sargent-Welch mechanical vacuum pump. Above 1 mm Hg, pressures were monitored by a mercury U-tube manometer and below 1 mm Hg by a General Electric Thermocouple Vacuum Gauge. Power was

applied to the heater tapes and adjusted until the desired isothermal condition was reached on the inner body. Simultaneously, cooling water flow rates were adjusted so that an isothermal condition was obtained on the outer body. Typically, temperature variation across either of the bodies ranged from .5-1.1°C (1-2°F) once steady state conditions were reached, which took about 2 hours. The data then taken were: thermocouple readings on the inner and outer bodies, voltage and current in each heater tape circuit, and air pressure within the test space. These raw figures were converted to inner and outer body temperatures and total power consumed (i.e., total heat transfer rate, assuming negligible power loss in the leads to the heater tapes).

The natural convection heat transfer must be obtained from the total heat transfer by subtracting off the radiation between the bodies and conduction down the stem. This correction was made by evacuating the system over a period of two days to pressures in the range of 3-13 Pa (25-100 microns Hg), where convection presumably does not occur [37]. Fifteen heat transfer data points were taken in this pressure range with temperature differences between the bodies ranging from 11.1-47.2°C (20-85°F). A plot of heat transfer against temperature difference resulted in a straight line. The equation of this line was then used in subsequent tests to remove radiation and stem conduction contributions.

Seventy-seven data points were taken with the cylindrical inner body and 26 with the cubical inner body. The data were reduced to the form shown in Appendix III on a Texas Instruments SR-40 calculator. The data were then further reduced and correlated by a Fortran IV program on the Xerox Sigma 7 computer.

Thirteen temperature profile sets were collected also. In these measurements, the temperature probe was inserted into the test space until it contacted the inner body. It was then withdrawn in small increments until the probe tip was flush with the wall of the test space. The thermocouple voltage and distance along the traverse were recorded at each step of the withdrawal. A second Fortran IV program was used to convert the voltages to temperatures and then calculate dimensionless temperatures and radii (see Figure 3.1):

$$T^* = \frac{T - T_{\text{outer body wall}}}{T_{\text{inner body wall}} - T_{\text{outer body wall}}}$$

$$r^* = \frac{\text{distance from outer body wall}}{\text{local gap between inner and outer wall}} .$$

Plots were then made of T^* against r^* for the various probe angles and experimental conditions.

Existing subroutines [33] were used to calculate the viscosity, heat capacity at constant pressure, and thermal conductivity of air. The density and coefficient of thermal expansion of air were calculated from the ideal gas law. In forming the dimensionless groups used to

correlate the data, no corrections were made in the air property values for non-standard pressure, except of course in the case of density. This is rigorously correct for the coefficient of thermal expansion and constant pressure heat capacity of an ideal gas [9]. It has been found very nearly correct for viscosity and thermal conductivity at pressures above 1 mm Hg, where the flow is viscous, not molecular [34-36]. No convection heat transfer was observed at pressures below 1 mm Hg, where pressure corrections to property values would become necessary. All property values were evaluated at the arithmetic mean fluid temperature:

$$T_m = \frac{T_o + T_i}{2} .$$

CHAPTER IV

HEAT TRANSFER AND TEMPERATURE PROFILE RESULTS

The heat transfer data taken in this investigation have been correlated in terms of the dimensionless parameters which are obtained from the nondimensional form of the governing equations of mass, momentum, and energy. The independent dimensionless parameters used here are the Rayleigh number, a correction for geometry, and a dimensionless density correction. The data include 70 data points taken over the pressure range of 2760-86,180 Pa (20-646.4 mm Hg) by the present author and 126 data points taken at local atmospheric pressure (86,180 Pa) previously by Warrington [33]. These two data sets will be referred to as "variable density" and "constant density" data, respectively. It should be noted that there is some variation (.97-1.06 kg/m^3) in fluid density in the latter data also as the temperature changes. This second group of data includes a third geometry, sphere-cube (inner body-outer body), in addition to the geometries described in Chapter III. There are also several sizes of inner body included in Warrington's data for each geometric class. The ranges of correlating parameters, pressures, and geometries used in the correlations are tabulated in Table 4.1. Many different correlations were tried. Those which will be discussed below are:

$$Nu_\delta = C_1 Ra_\delta^{C_2} \qquad (4.1)$$

$$Nu_\delta = C_1 Ra_\delta^{*C_2} \qquad (4.2)$$

$$Nu_\delta = C_1 Ra_\delta^{C_2} (L/R_i)^{C_3} \qquad (4.3)$$

$$Nu_b = C_1 Ra_b^{C_2} \qquad (4.4)$$

TABLE 4.1

RANGE OF GEOMETRIES AND CORRELATING PARAMETER

Type of Data	Inner Body	Dimensions (cm)	Range of Ra_L
Variable density	Cylinder	11.43 x 22.61	$1.7 \times 10^3 - 1.9 \times 10^6$
	Cube	12.7	$1.1 \times 10^3 - 1.8 \times 10^6$
Constant density	Sphere	11.43	$7.5 \times 10^5 - 5.1 \times 10^6$
		17.78	$4.6 \times 10^5 - 1.8 \times 10^6$
		22.86	$1.7 \times 10^5 - 4.4 \times 10^5$
	Cylinder	11.43 x 16.13	$9.0 \times 10^5 - 3.8 \times 10^6$
		17.78 x 22.61	$3.4 \times 10^5 - 1.2 \times 10^6$
		17.78 x 20.57	$3.4 \times 10^5 - 1.3 \times 10^6$
		11.43 x 22.61	$7.6 \times 10^5 - 2.9 \times 10^6$
	Cube	10.16	$9.8 \times 10^5 - 4.5 \times 10^6$
		12.70	$5.6 \times 10^5 - 2.6 \times 10^6$
		16.26	$3.2 \times 10^5 - 1.1 \times 10^6$

$$Nu_b = C_1 Ra_b^{*C_2} \tag{4.5}$$

$$Nu_b = C_1 Ra_b^{C_2} (L/R_i)^{C_3} \tag{4.6}$$

$$Q = C_1 Ra_\delta^{C_2} \tag{4.7}$$

$$Q = C_1 Ra_\delta^{*C_2} \tag{4.8}$$

$$Q = C_1 Ra_\delta^{C_2} (L/R_i)^{C_3} \tag{4.9}$$

$$Nu_\delta = C_1 Ra_\delta^{C_2} \left(\frac{\rho}{\rho_{atm}}\right)^{C_3} \tag{4.10}$$

$$Nu_\delta = C_1 Ra_\delta^{C_2} \left(\frac{\rho}{\rho_{atm}}\right)^{C_3} \left(\frac{L}{R_i}\right)^{C_4} \tag{4.11}$$

$$Nu_\delta = C_1 Ra_\delta^{1/4} \left(\frac{\rho}{\rho_{atm}}\right)^{C_2} \tag{4.12}$$

$$Nu_\delta = C_1 Ra_\delta^{1/4} \tag{4.13}$$

$$Nu_\delta = C_1 Ra_\delta^{1/4} \left(\frac{L}{R_i}\right)^{C_2} \tag{4.14}$$

where L is the gap width between hypothetical concentric spheres of volumes equal to those of the inner and outer bodies, R_i is the radius of such an inner sphere, b is the distance traveled by the boundary layer along the inner body assuming no flow separation, ρ and ρ_{atm} are the air density in the experiment and at standard atmospheric pressure, and δ is any one of three different gap widths described below. In addition to these correlations, the data were tested against correlations recommended by Warrington [33]. Chapter V is devoted to developing and testing correlations based on the method of Raithby and Hollands [4].

Three different methods were used to determine the characteristic gap width to be used in formulating the parameters Ra_δ and Nu_δ. L is as

defined above. L' is the average gap width obtained by integrating the local gap width over the surface of the inner body. For cubical and spherical inner bodies, this local gap is measured along a ray originating in the center of the enclosure. For cylindrical inner bodies, the local gap is defined as diagrammed in Figure 4.1. L" is the gap width between hypothetical spheres of surface areas equal to those of the inner and outer bodies. Thus L emphasizes the bulk sizes of the bodies, L' emphasizes the distance between the bodies, and L" emphasizes the areas on which the heat transfer takes place.

Figure 4.2 is a plot of the heat transfer data used in this investigation, including data of Warrington [33]. For clarity, only about one third of Warrington's data is plotted here. Figure 4.2 demonstrates considerable geometric dependence of heat transfer, particularly in Warrington's data. The equal-volume gap width, L, was used in formulating the dimensionless groups of Figure 4.2. Table 4.2 lists least-squares curve-fits of all the data for various correlations. The Nusselt number correlates the data better than the ratio of q_{conv}/q_{cond}. Of the three gap widths used, L gives slightly better results in the Nu correlations, while L" has a slight edge in Q correlations. In neither case is the advantage significant, and L-based correlations will be reported hereafter, except where some particular advantage or physical significance is associated with other gap widths.

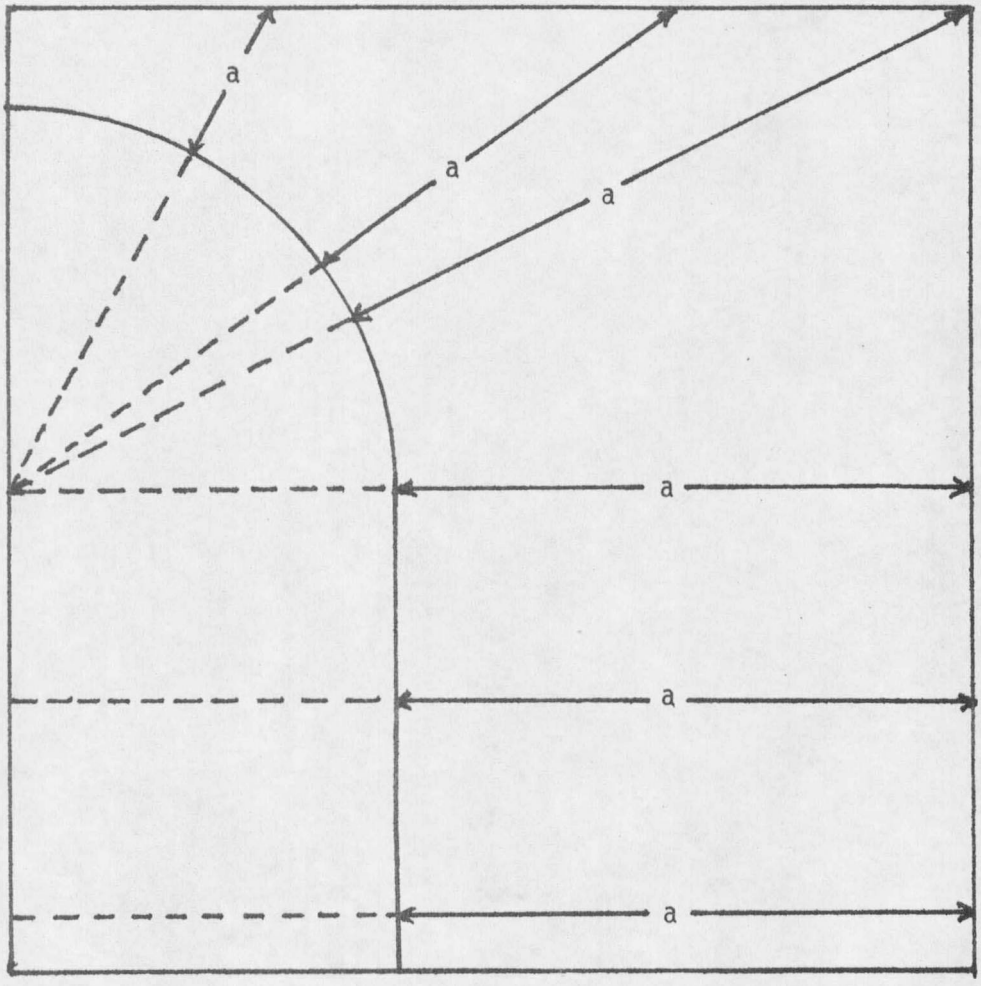


Figure 4.1 Local Gap Width a for the Cylinder-Cube Geometry

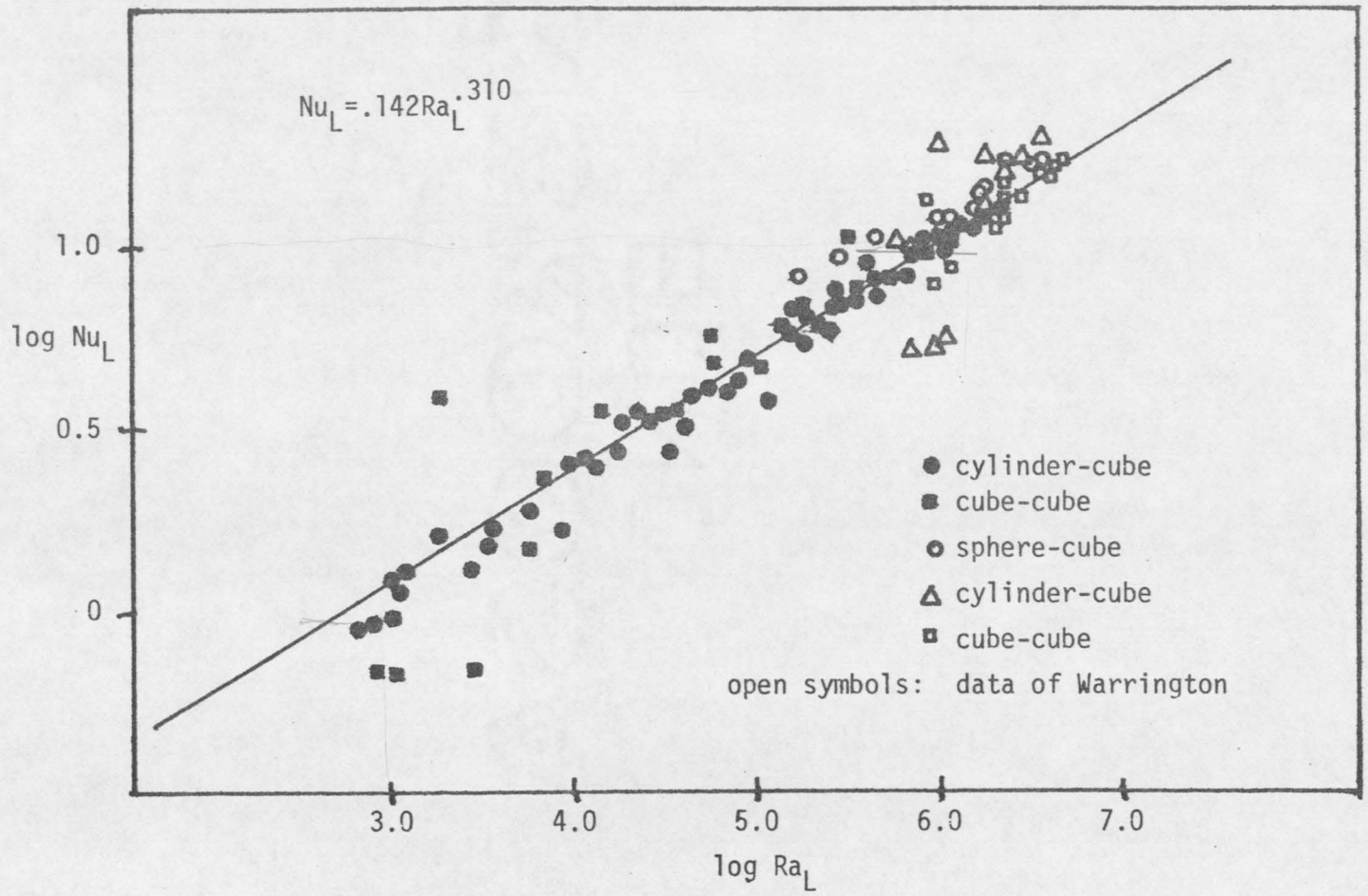


Figure 4.2 All of the Heat Transfer Data: Nu_L vs. Ra_L

TABLE 4.2

CORRELATION EQUATIONS FOR ALL DATA

Equation Form	δ	Empirical Constants C_1	C_2	C_3	C_4	Average % Deviation	% of data within ±20% of equation
(4.1)	L	.123	.324			18.91	70.41
	L'	.129	.321			18.96	68.88
	L"	.122	.325			18.93	70.92
(4.2)	L	.132	.317			17.86	71.94
	L'	.136	.315			17.93	71.94
	L"	.129	.319			17.91	70.92
(4.3)	L	.133	.317	.303		17.89	71.43
	L'	.137	.315	.301		17.96	71.43
	L"	.130	.319	.299		17.95	71.43
(4.4)		.186	.301			18.85	69.90
(4.5)		.139	.317			17.95	70.92
(4.6)		.140	.315	.253		17.88	71.94

TABLE 4.2 (Continued)

Equation Form	δ	Empirical Constants C_1	C_2	C_3	C_4	Average % Deviation	% of data within ±20% of equation
(4.7)	L	.0581	.318			18.02	69.39
	L'	.0545	.315			20.37	66.33
	L"	.0509	.317			17.79	71.43
(4.8)	L	.0721	.300			21.80	51.53
	L'	.0649	.300			24.01	47.96
	L"	.0607	.302			21.71	58.67
(4.9)	L	.0567	.321	-.107		17.70	75.00
	L'	.0542	.315	-.0322		20.12	66.84
	L"	.0506	.317	-.0373		17.54	72.96
(4.13)	L	.364				28.63	54.59
	L'	.372				27.97	55.10
	L"	.379				28.97	54.08
(4.14)	L	.317	.360			21.47	58.16
	L'	.327	.341			21.54	61.22
	L"	.331	.342			21.92	59.18

As Warrington [33] has pointed out, even over this wide range of enclosure geometries, the heat transfer results are correlated as well by an infinite atmosphere type of correlation as by one based on the enclosure geometry. Correlations based on b, the length of the inner boundary layer, provide results as satisfactory as ones based on gap widths. One of the better correlations, equation (4.6), takes into account both the boundary layer and gap width dimensions individually. When the two lengths are combined into a single parameter, Ra_b^* (equation (4.5)), the correlation is only slightly worse. The enclosure geometry is not entirely insignificant, however, as evidenced by the much higher rise in the average deviation, from 17.95 to 18.85 percent, when the enclosure is ignored in equation (4.4).

The correlations formulated with Q, equations (4.7-4.9), are affected differently by the inclusion of the geometry parameter. Equation (4.8), based on Ra_b^*, produces for all gap widths considerably greater error than either equation (4.7) or (4.9). When L/R_i is included as an independent parameter in equation (4.9), the best fit, with L", has an average deviation of 17.54 percent, whereas equation (4.7), also based on L" but with no geometric correction, has an average deviation of 17.79 percent. Further, the exponent on the L/R_i factor in equation (4.9) is quite small, which signifies a small geometric dependence. Thus in forming the ratio of convection to hypothetical conduction heat transfer, the area available for heat transfer is the important parameter, and the

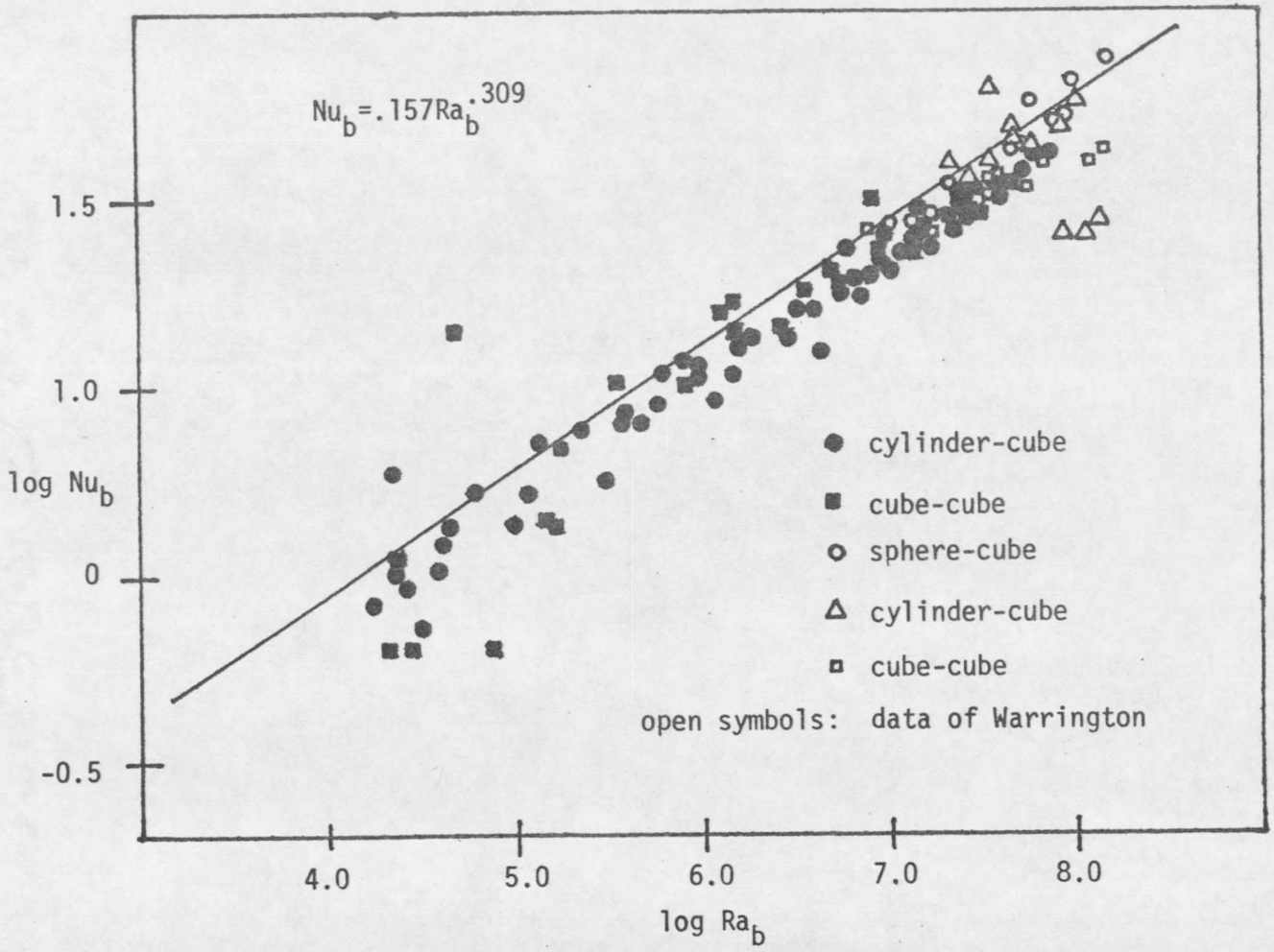


Figure 4.3 All of the Heat Transfer Data: Nu_b vs. Ra_b

geometric configuration is of small importance. It seems likely that the geometric variation is similar in its effect upon the rates of convection and conduction in the stagnant fluid.

An additional insight into the significance of the geometric correction may be gained by inspection of the tabulations in Table 4.2 for equation forms (4.1), (4.2), (4.3), (4.13), and (4.14). When the governing differential equations of continuity, momentum, and energy are cast in dimensionless form, it can be shown [5] that the expected correlation for overall heat transfer is

$$Nu_a = C\ Ra_a^{1/4}$$

where a is an appropriate dimension. The corresponding equation for an enclosure geometry is equation (4.13). Table 4.2 shows that this correlation does not work well with the present data. Equation (4.1) works much better, and it is found that the preferred exponent on the Rayleigh number is .32, rather than the classically expected .25. This deviation is among the more significant results of this investigation, and attempts will be made to explain it.

At least part of this deviation is due to the geometric influence, as may be seen in several ways. First, equations (4.2) and (4.3), which include geometric corrections, either in Ra* or independently, deviate less in the Rayleigh number exponent than does equation (4.1). Also, equation (4.14), which contains a strong independent geometric correction

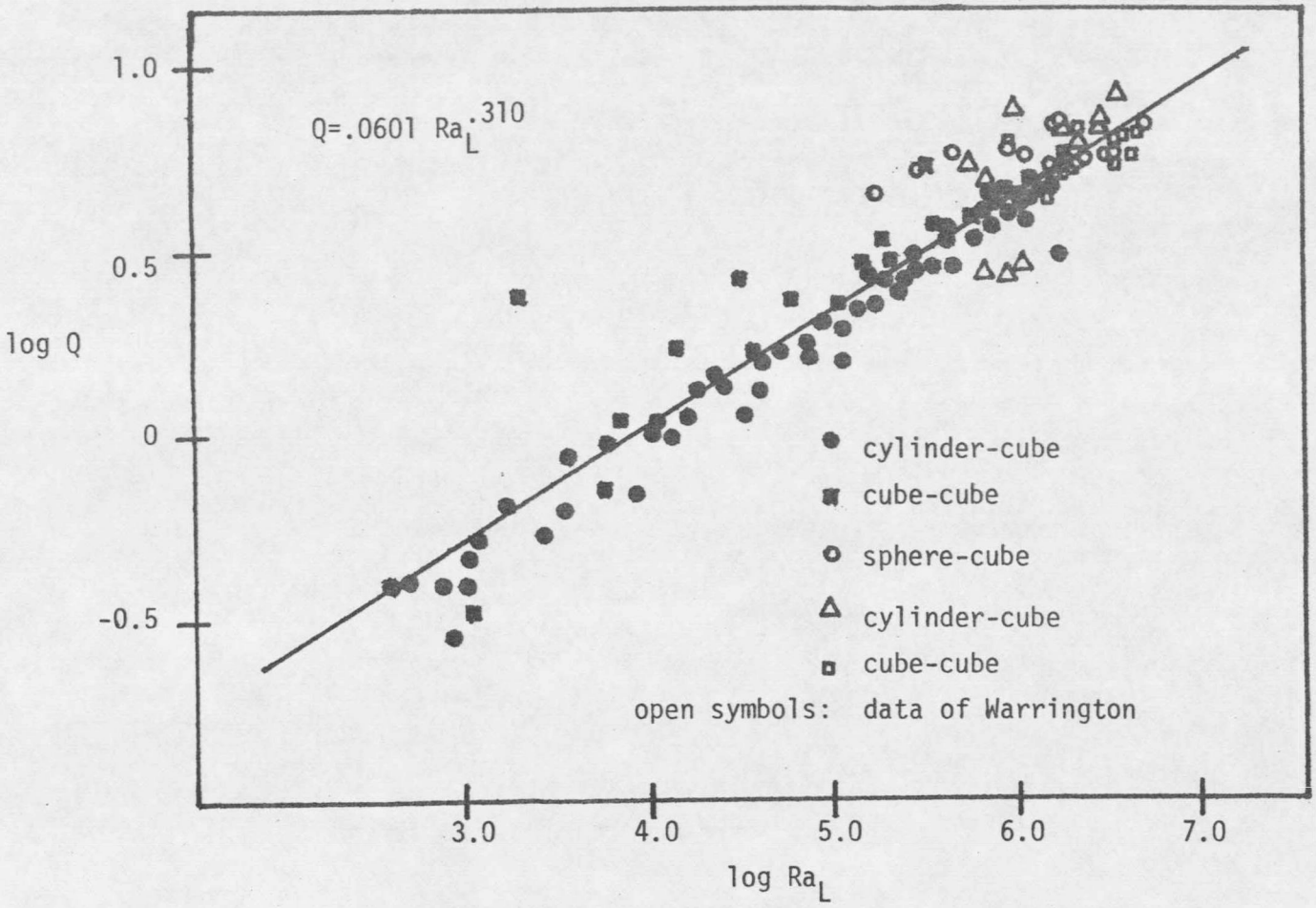


Figure 4.4 All of the Heat Transfer Data: Q vs. Ra_L

but retains the .25 power on Ra, correlates the data much better than equation (4.13). This improvement amounts to most of the improvement achieved by allowing the exponent on Ra to vary freely. Of the equations discussed so far, the best correlations with each dependent dimensionless parameter are:

$$Nu_L = .132Ra_L^{.317}\left(\frac{L}{R_i}\right)^{.303} \qquad (4.15)$$

$$Nu_b = .145Ra_b^{.315}\left(\frac{L}{R_i}\right)^{.253} \qquad (4.16)$$

$$Q = .0506Ra_L^{.317}\left(\frac{L}{R_i}\right)^{-.0373} \qquad (4.17)$$

with average deviations of 17.86, 17.88, and 17.54 percent, respectively.

Since this work, as explained in Chapter II, is a continuation of research initiated by Warrington [33], his recommended correlations for air were tested against data taken by the present author. The better correlations were:

$$Nu_L = .425Ra_L^{.234}\left(\frac{L}{R_i}\right)^{.498} \qquad (4.18)$$

$$Nu_L = .612Ra_L^{.207}\left(\frac{L}{R_i}\right)^{.508} \qquad (4.19)$$

$$Nu_L = .173Ra_L^{*\ .299} \qquad (4.20)$$

$$Nu_b = .570\ Ra_b^{.228}\left(\frac{L}{R_i}\right)^{.162} \qquad (4.21).$$

No correlations with Q fit the present data acceptably. Equation (4.18)

is a correlation recommended for all fluids and all geometries. The other correlations are specifically for air. The results of these correlations are presented in Table 4.3. It is interesting to note that equation (4.18), recommended for all fluids, works better here than the corresponding equation for air, equation (4.19). Again the correlations with higher Ra exponents give better fits to these data. It is then not surprising that equation (4.20) correlates the data best among these. There are two possible reasons why Warrington's correlations do not work well on the present data, one statistical and the other physical. Warrington's air data cover a relatively small range of Ra (see Figure 4.2). Also there is considerable scatter in these data [33]. Therefore, the correlations presented for air may not be highly accurate. As an illustration of this, in Warrington's correlations of the forms (4.1-4.a), the exponent on Ra varies over .171-.299. In the present data, this variation is .300-.325. The other possibility is that there is something physically different about variations in Ra caused primarily by changing the fluid density, as in the present experiments, and variations due to changing the gap width and/or temperature difference as Warrington did. This will be discussed in greater detail below.

Correlations were also generated from the data taken in this investigation alone. These correlations are presented in Table 4.4, for equation forms (4.1)-(4.9), (4.13), and (4.14). Table 4.4 is thus equivalent to Table 4.2, except that it is for the variable density data

TABLE 4.3

FIT OF PRESENT DATA TO PREVIOUS CORRELATIONS

Equation	Average % Error	% of data within ±20% of equation
(4.18)	41.39	35.71
(4.19)	51.65	34.29
(4.20)	17.78	75.71
(4.21)	24.33	64.29

TABLE 4.4

CORRELATION EQUATIONS FROM THE VARIABLE DENSITY DATA ALONE

Equation Form	δ	Empirical Constants				Average % Deviation	% of data within ±20% of equation
		C_1	C_2	C_3	C_4		
(4.1)	L	.142	.310			10.99	84.29
(4.2)	L	.137	.310			11.02	84.29
(4.3)	L	.192	.310	-2.486		11.62	85.71
(4.4)		.157	.309			10.98	84.29
(4.5)		.152	.308			10.99	84.29
(4.6)		.203	.310	-2.268		11.62	85.71
(4.7)	L	.0601	.310			14.31	80.00
(4.8)	L	.0582	.309			14.63	78.57
(4.9)	L	.145	.310	.7.20		11.62	85.71
(4.13)	L	.311				20.47	68.57
(4.14)	L	.371	-2.454			17.32	80.00

only. It is striking that, in forms (4.1)-(4.9), any inclusion of the geometric effect in the correlation actually worsens the results. Clearly the variation between the two geometries used here (see Chapter III) is insignificant in the overall heat transfer rate. Again the boundary layer length correlations are nearly as accurate as those based on gap width. This is somewhat more surprising in this case, because the thermal boundary layer becomes thicker at low Rayleigh numbers and the infinite atmosphere approximation should become less accurate. But since the boundary layer length is an easy dimension to define, a correlation based on this length alone is useful.

The Q correlations were not as satisfactory for the variable density data. In this case, though, accuracy was remarkably improved by including an independent geometric parameter in the correlation. The best of the above correlations of each type are:

$$Nu_L = .142Ra_L^{.310} \qquad (4.22)$$

$$Nu_b = .157Ra_b^{.309} \qquad (4.23)$$

$$Q = .145Ra_L^{.310}\left(\frac{L}{R_i}\right)^{-7.20} \qquad (4.24)$$

with average deviations of 10.99, 10.98, and 11.62 percent, respectively. Equations (4.22) and (4.23) are plotted on Figures 4.2 and 4.3, respectively.

Equations (4.22)-(4.24) were tested against all of Warrington's air data as an additional check on their validity. These equations resulted in average deviations of 23.09, 22.01, and 2206 (sic) percent, respectively. The very large error for equation (4.24) signifies that the geometric correction calculated from the present data alone is unreliable. With only two geometries used, the range of L/R_i was not great enough to produce an accurate dependence. It is recommended that, in variable-density problems with widely varying geometries, equation (4.22) or (4.23) be used. These two equations do not fit the data particularly well at pressures near atmospheric, however. (Warrington's data were taken at 86,100 Pa (646 mm Hg), which is local atmospheric pressure where these experiments were performed.) It is therefore further recommended that, in problems near atmospheric pressure, correlations of Warrington [33] be used.

Since equation (4.24) was entirely unsatisfactory in correlating the previous data, the following equation from Table 4.4 was tried:

$$Q = .0601 Ra_L^{.310} \qquad (4.25)$$

The resulting average deviation was 19.17 percent, a somewhat better fit than either equation (4.22) or (4.23). Equation (4.25) is plotted on Figure 4.4.

The present data from the cylinder-cube and cube-cube experiments are plotted in Figures 4.5 and 4.6, respectively. The recommended

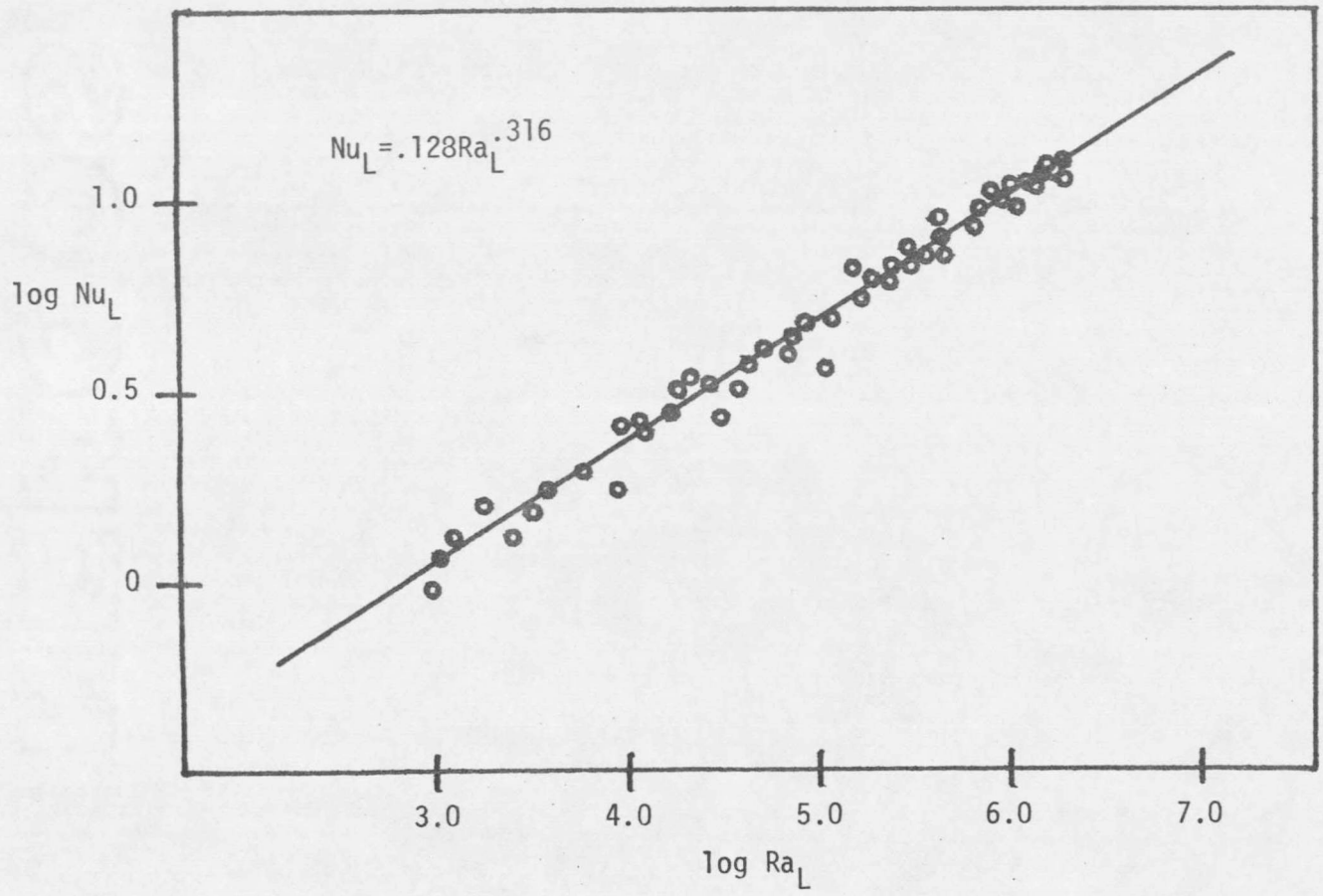


Figure 4.5 Variable-Density Data, Cylinder-Cube Geometry

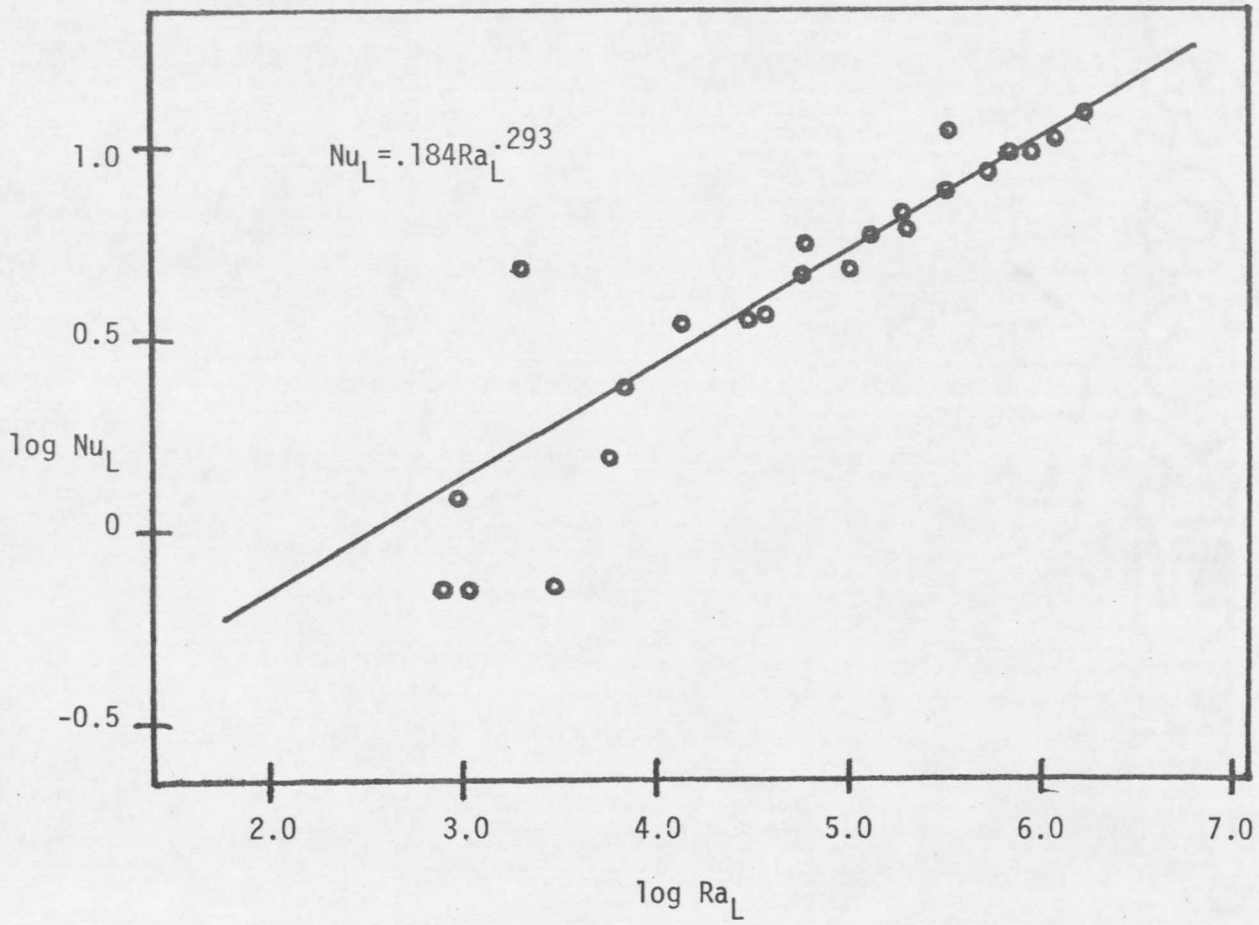


Figure 4.6 Variable-Density Data, Cube-Cube Geometry

correlations for the cylinder-cube data are:

$$Nu_L = .128Ra_L^{.316} \qquad (4.26)$$

$$Nu_b = .136Ra_b^{.316} \qquad (4.27)$$

$$Q = .0516Ra_L^{.316} \qquad (4.28).$$

In all cases the average deviation is 8.08 percent, and 92 percent of the data fall within ±20 percent of the equation. For the cube-cube data, the recommended correlations are:

$$Nu_L = .184Ra_L^{.293} \qquad (4.29)$$

$$Nu_b = .210Ra_b^{.293} \qquad (4.30)$$

$$Q = .0885Ra_L^{.293} \qquad (4.31).$$

The average deviation in each case is 19.85 percent, with 80 percent of the data falling within ±20 percent of the equation. Clearly the correlations used so far, which are based on the assumed smooth boundary layer flow over the heated body or on behavior similar to a spherical body of similar size, do not work well on the cubical inner body. The likely source of error is that buoyant forces, which act vertically, do not act in the direction of flow along the top and bottom faces, which thus produces a situation quite different from that of a rounded object. This subject will be taken up in greater detail in Chapter V.

LOW DENSITY RESULTS

Figure 4.7 is a plot of all the data taken in the present investigation, over the pressure range of 2320-85870 Pa (17.4-643.4 mm Hg). There is no discernible break in the slope. When the data above and below 26660 Pa (200 mm Hg) are correlated separately, the following results are obtained:

$$Nu_{L''} = .143Ra_{L''}^{.317}, \quad P \leq 26660 \text{ Pa} \qquad (4.32)$$

$$Nu_{L''} = .158Ra_{L''}^{.303}, \quad P > 26660 \text{ Pa} \qquad (4.33)$$

with average deviations of 15.03 and 6.42 percent, respectively. It is expected that the slope would decrease at lower Rayleigh numbers (10.13) but this is not evident here. The slight increase in slope observed is probably not significant, because the scatter in the data becomes larger as the heat transfer rate decreases. At lower Ra, the convection heat transfer is much smaller than the radiation contribution, so when the radiation is subtracted from the total, the result (convection) contains a fairly large error. Since the Ra exponent is only slightly changed, the range of data in Figure 4.7 will be considered a single regime hereafter.

It has been hypothesized above that the Rayleigh number and geometric corrections alone do not adequately correlate natural convection over the present range of lower pressures. To test this hypothesis, a

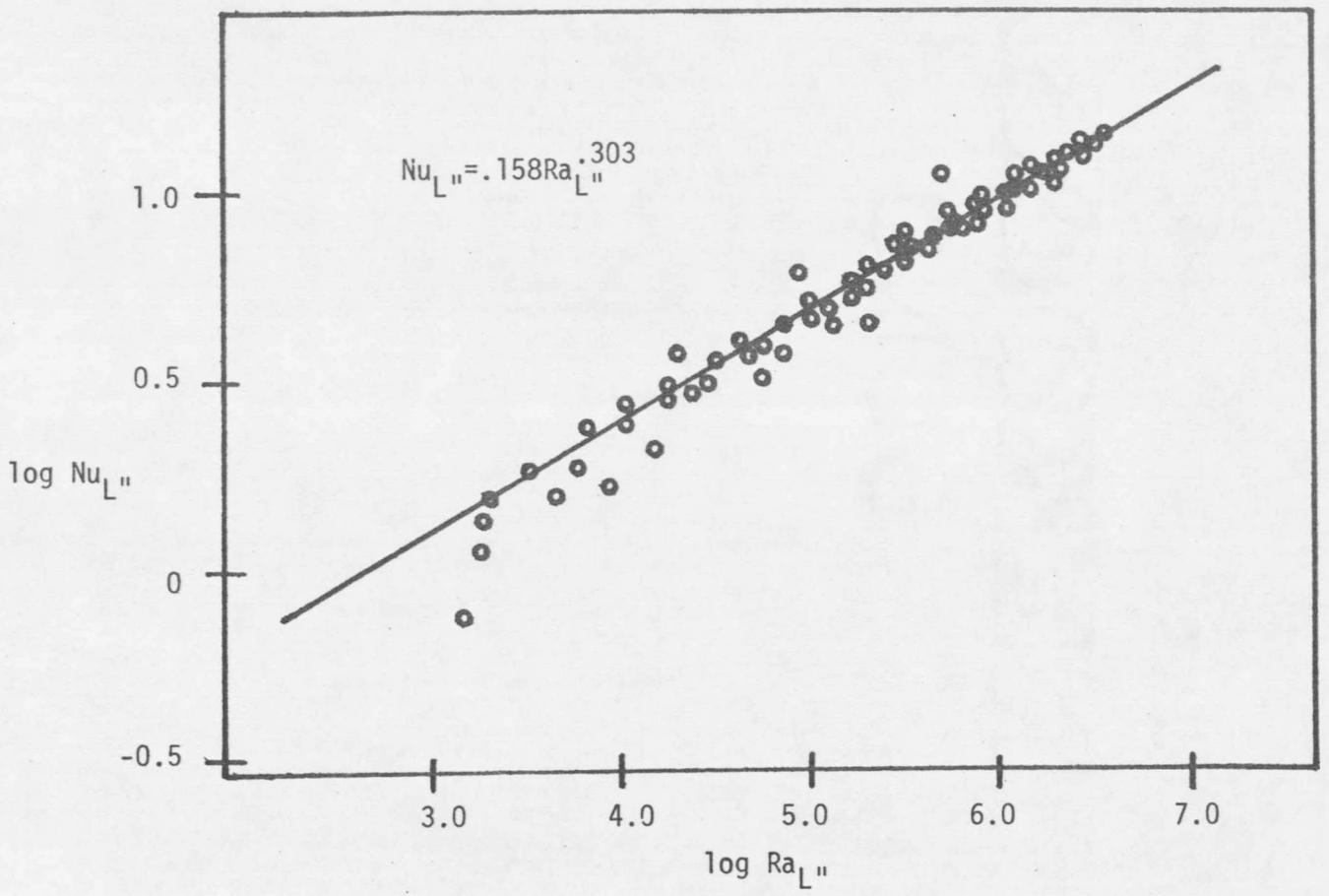


Figure 4.7 All of the Variable-Density Data: $Nu_{L"}$ vs. $Ra_{L"}$

dimensionless density parameter was inserted into the basic correlations (equations (4.10)-(4.12)). The results are presented in Table 4.5. Of primary importance is the result that equation (4.12) correlates the data as well as any other, indeed slightly better. The only way in which equation (4.12) differs from the classical correlation (equation (4.13)) is in the inclusion of the density parameter. This modification alone is enough to affect the great improvement in the correlation shown in Table 4.5. This is the most compelling evidence that the deviation of the Rayleigh number exponent from the expected .25 value is due to the variation in fluid density. Even equation (4.10), in which the Rayleigh number and density parameter are each allowed to vary freely, does not correlate as well as equation (4.12), in which Ra is fixed at the classical one fourth power. Equation (4.11), in which the geometric parameter is also included, slightly worsens the correlation. As noted above, however, the range of geometries in this data is quite small, and thus the calculated geometric effect is not very reliable.

The classical correlation alone, $Nu_L = .311 Ra_L^{1/4}$, correlates the data with an average deviation of 20.47 percent. The modification of the exponent in equation (4.1),

$$Nu_L = .142 Ra_L^{.310},$$

and the inclusion of the density parameter in equation (4.12),

$$Nu_L = .342 Ra_L^{1/4} (\rho/\rho_{atm})^{.129},$$

each reduce the average deviation by about half, to 10.99 and 10.92

TABLE 4.5

DENSITY-CORRECTED CORRELATIONS FOR THE VARIABLE DENSITY DATA

Equation Form	δ	Empirical Constants C_1	C_2	C_3	C_4	Average % Deviation	% of data within ±20% of equation
(4.1)	L	.142	.310			10.99	84.29
(4.3)	L	.192	.310	-2.486		11.62	85.71
(4.10)	L	1.475	.148	.328		11.59	85.71
(4.11)	L	1.747	.155	.314	-2.201	11.88	85.71
(4.12)	L	.342	.129			10.92	84.29
(4.13)	L	.311				20.47	68.57
(4.14)	L	.378	-2.454			17.32	80.00

percent, respectively. Either equation (4.1) or (4.12) is easy to use, with the advantage going to (4.1), since it contains one fewer parameter. It is the author's opinion that both of these equations may be used confidently in reduced-pressure heat transfer calculations, as long as pressures are within the present range and the geometries are not radically different from these.

The success of the density correction introduced has been further tested with Warrington's data. These data were taken at local atmospheric pressure, which may be viewed as a partial "vacuum" at 86000 Pa (645 mm Hg, or .85 atm). All of the present data and Warrington's data were correlated with equations (4.10)-(4.14), and the results are presented in Table 4.6. Equation (4.13) correlated all the data with an average deviation of 28.63 percent. The geometric correction in equation (4.14) improved this figure to 21.47 percent, while the density correction in equation (4.12) did slightly better with an average deviation of 19.76 percent. This is additional evidence that the change in density is the major influence in the exponent of the Rayleigh number.

The entries in Tables 4.5 and 4.6 for equation (4.10) are striking in comparison. When this equation is used to correlate the variable-density data only (Table 4.5), the Rayleigh number exponent is .148. This demonstrates that the major variant in the Rayleigh number in the present experiments was indeed the density, because the Ra dependence is much weaker when the density dependence is included independently.

TABLE 4.6

DENSITY-CORRECTED CORRELATIONS FOR ALL DATA

Equation Form	δ	Empirical Constants				Average % Deviation	% of data within ±20% of equation
		C_1	C_2	C_3	C_4		
(4.1)	L	.123	.234			18.91	70.41
(4.3)	L	.132	.317	.303		17.86	71.94
(4.10)	L	.145	.313	.0256		18.97	70.92
(4.11)	L	1.969	.131	.408	.571	17.53	70.41
(4.12)	L	.359	.151			19.76	70.41
(4.13)	L	.364				28.63	54.59
(4.14)	L	.317	.360			21.47	58.16

In the corresponding entry in Table 4.6, the Ra dependence is back to .313 power, and the density parameter dependence is quite small at .0256 power. This is merely an illustration of the strong slanting of the data towards the atmospheric case, i.e., Warrington's 126 data points were all taken at atmospheric pressure, whereas only 70 data points were taken over the entire pressure range. The correction for both density and geometry, equation (4.11), does yield further improved results (see Table 4.6), with an average deviation of 17.53 percent, but it is questionable whether the additional gain in accuracy over equation (4.10) or, indeed, over equation (4.3) (see Table 4.2) justifies the additional computational effort. It is clear that additional data with other geometries over the entire range of pressures would be useful to fully evaluate the relative importances of geometric and density corrections to the basic correlations.

In summary, and realizing that the geometric effect remains unclear at low pressures, (<26660 Pa), the following correlations are recommended over the range of pressures encountered here:

$$Nu_L = .142Ra_L^{.310} \qquad (4.34)$$

$$Nu_L = .342Ra_L^{1/4}(\rho/\rho_{atm})^{.129} \qquad (4.35).$$

It should be noted that the primary mode of heat transfer at low pressures is radiative, which is geometry dependent. Therefore, even if

geometry does not significantly affect these correlations, it will have a large effect on overall rates of heat transfer.

TEMPERATURE PROFILE RESULTS

Temperature profiles between the cylinder and the enclosing cube over the range of experimental pressures are displayed in Figures 4.8-4.11. Immediately evident is the thickening of the boundary layer on the inner body at lower pressures (Figures 4.8, 4.9). At higher pressures (Figures 4.8, 4.11), the five regions reported by Warrington [33] are observed: a steep drop at the inner body, an inner transition region, a level zone with perhaps a slight temperature inversion, an outer transition zone, and a fairly steep drop again at the outer wall. These five zones are convincingly present only for the 34° and 80° probes (see Chapter III). In every case the 0° and 160° profiles have no points of inflection, and a steep drop at the inner wall slowly levels off to a less drastic monotonic decrease over the remainder of the gap. There is never a region of constant temperature as with the 34° and 80° probes. This result agrees well with analytical results of Mack and Hardee [29] and experiments of Scanlan, Bishop, and Powe [25] for concentric spheres. The velocity profile at 160° presented by Mack and Hardee indicates very little convective activity; this is also supported by flow visualization pictures of Warrington [33,40]. The 160° temperature profile of Mack and Hardee at Ra=1000 is also a monotonically

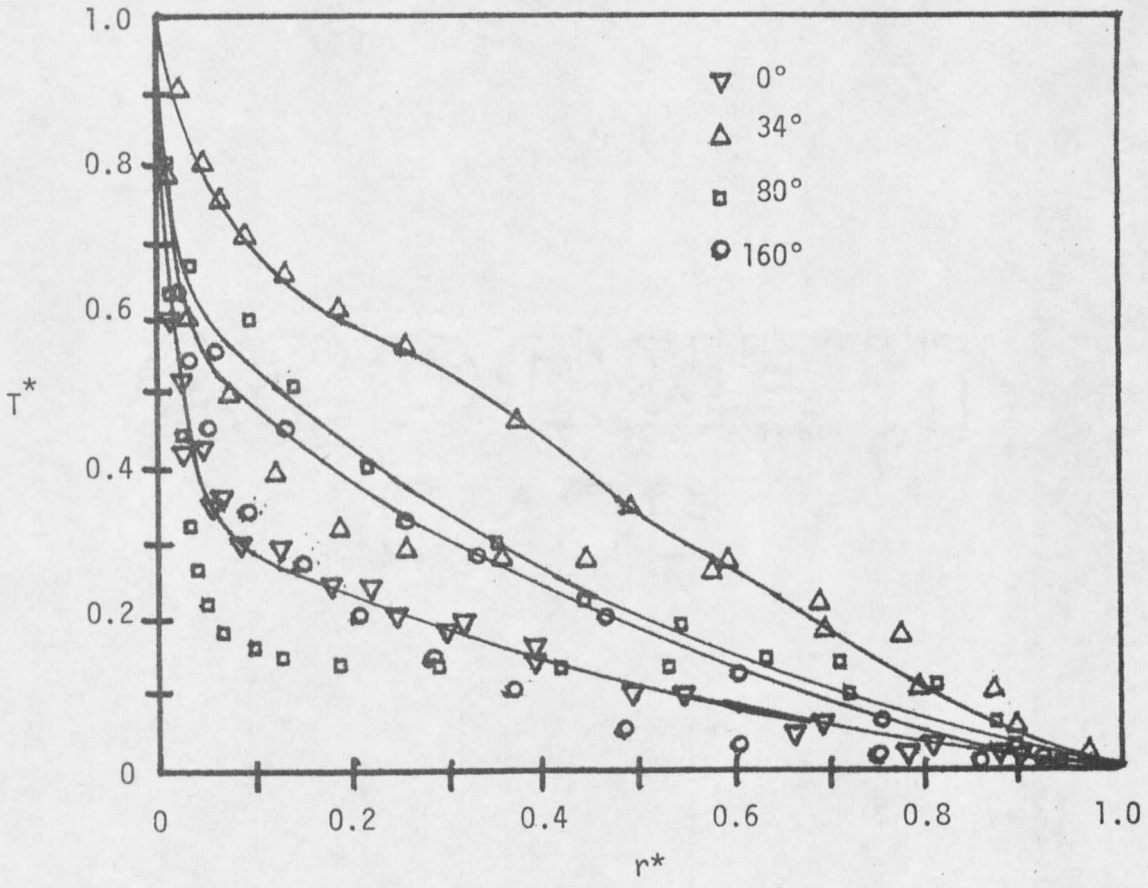


Figure 4.8 Temperature Profile Data at Two Different Pressures: Solid Lines--ΔT = 23.3°C (42.0°F), Pressure = 16.3 mm Hg; Open Symbols--ΔT = 20.7°C (37.2°F), Pressure = 641.9 mm Hg.

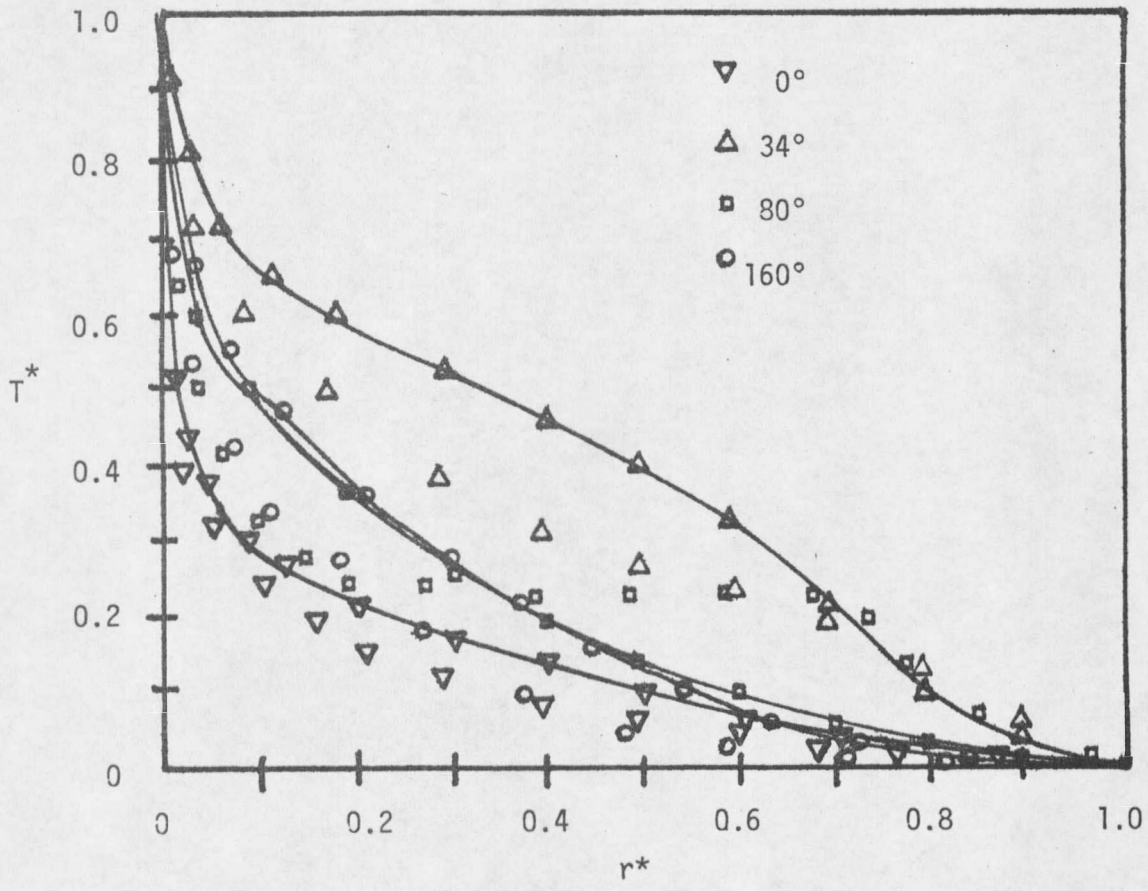


Figure 4.9 Temperature Profiles at Two Different Pressures: Solid Lines--ΔT=30.2°C (54.4°F), Pressure=48.0 mm Hg; Open Symbols--ΔT=18.7°C (33.6°F), Pressure =149.6 mm Hg.

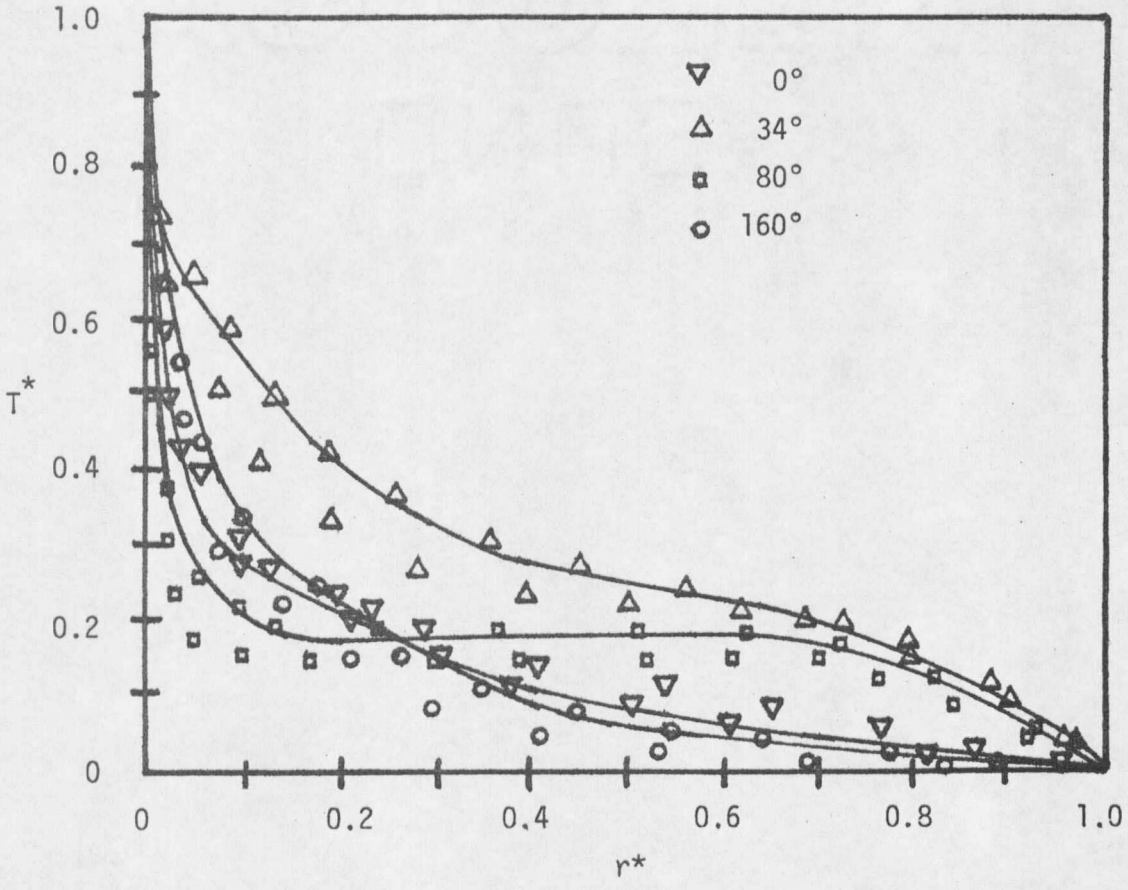


Figure 4.10 Temperature Profile Data at Two Different Pressures: Solid Lines--ΔT=23.8°C (42.8°F), Pressure=248.8 mm Hg; Open Symbols--ΔT= 22.9°C (41.3°F), Pressure=505.7 mm Hg.

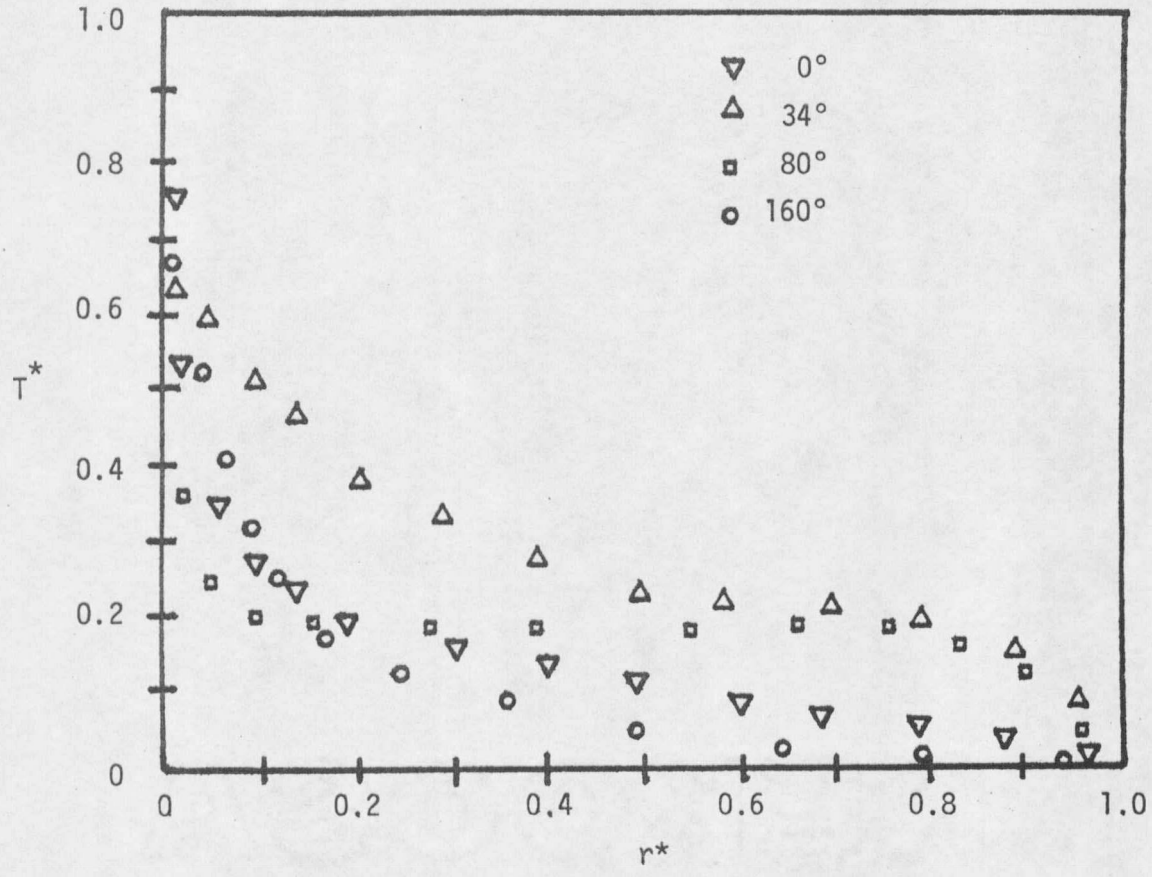


Figure 4.11 Temperature Profile Data:

ΔT=22.8°C (41.1°F),

Pressure=396.8 mm Hg.

decreasing function of the same form as the 160° low pressure profiles in Figures 4.8-4.9. At higher Rayleigh numbers the initial drop becomes steeper, and the high-temperature region becomes smaller. These are manifestations of the decrease in boundary layer thickness at high Rayleigh numbers. The monotonic decrease in the temperature profile at 160° indicates that heat transfer at this position is nearly pure conduction [33,29].

The form of the profiles at 0° is similar to that at 160°, but for a different reason. Warrington [33] reported explanations of McCoy et al [41], Bishop et al [42], and Scanlan et al [25], that the form of the 0° profile is due to a corner eddy and flow separation near the top of the inner body. This effect is apparently present over the entire pressure range of the present experiments, because the form of the 0° profile in Figures 4.8-4.11 is virtually unchanged. If the flow were smooth and attached to the top of the inner body, Mack and Hardee's [29] analysis would predict a downward, rather than upward, concavity on the profile for 0°. Warrington found this to be the case for fluids of higher Prandtl number (i.e., higher viscosity).

The ordering of the profiles vertically changes over the range of pressures. At low pressure, and excluding the anomalous behavior of the 0° profile, the ordering is as would be expected: 160° profile lowest and 34° profile highest. This demonstrates the heating of the fluid as it flows up the body. At higher pressures, Figure 4.8, this ordering is

maintained only extremely close to the inner wall and at distances well away from the inner wall. The probable explanation is that there is no well-defined boundary layer yet formed at the 160° position, and the heat transfer is largely conductive, as stated above. In all cases, the 34° profile is above the 80° profile, as would be expected.

The region of higher temperature near the inner body is much larger at the 34° position than at the 80° position. This corresponds to the increase in boundary layer thickness in the direction of flow, as would be expected. It is also possible that the outer body has an effect on the 34° profile. The 11.4x22.6 cm (4.5x8.9 in) cylinder used here fills most of the vertical space within the enclosure, so that the flow at 34° on the inner body may well be impeded by return flow along the top face of the outer body. Flow visualization data of Warrington [33] show that at the 34° position the corner eddy mentioned above has begun to form. There is thus a region of near stagnation close to the inner body, which would account for the anomalously linear inner transition at 34° in Figure 4.11. Farther away from the body the flow is again smooth and the expected leveling off of the profile between the inner and outer bodies occurs.

The 80° profile is the most idealized form. At this point in the flow, there is considerable distance between the inner and outer boundary layers, the boundary layer has had ample space to develop and stabilize, and there is no negative pressure gradient and resultant flow separation.

The slight temperature inversion in the 80° profile near the outer transition region is due to the small rotational motion of the fluid between the inner and outer boundary layers.

CHAPTER V

A MODIFICATION OF THE METHOD OF RAITHBY AND HOLLANDS FOR CUBICAL GEOMETRIES

The method of generating natural convection heat transfer correlations developed by Raithby and Hollands [4] is introduced in Appendix I. To summarize, the assumptions of the model are:

1. Laminar flow, with constant fluid properties;
2. Boundary layers are thin compared to the radius of curvature;
3. Linear temperature profile in the inner region of the boundary layer;
4. Insignificant acceleration forces in the inner region, so that viscous and buoyant forces balance; and
5. The ratio of buoyancy in the inner region to total buoyancy in the boundary layer depends on the Prandtl number only and not on geometry.

Assumptions 1 and 2 have been removed by further developments in the model [4,44].

There will be two sections to this chapter: an adaptation of Raithby and Hollands's result for concentric spheres to the present geometries, and a modification of the basic theory to account for convective flow around a cube. It is worth clarifying at the outset that this method always generates correlations of the form

$$Nu_a \text{ (or } Q) = C_1 Ra_a^{1/4} \cdot G \qquad (5.1),$$

where G is a correction for geometry.

CONCENTRIC SPHERES

The starting point for generating a correlation based on concentric spheres is equation (A1.16):

$$\bar{\Delta}_{i,o} = \frac{S_{i,o}}{\bar{C}_{i,o} Ra_{S_{i,o}}^{1/4}} \frac{\frac{1}{S_{i,o}} \int_0^{S_{i,o}} r_{i,o} dx_{i,o}}{\left[\frac{1}{S_{i,o}} \int_0^{S_{i,o}} \left(\frac{T_{i,o} - T_m(X_{i,o})}{\Delta T_r}\right)^{5/3} \left(\frac{g_{X_{i,o}}}{g}\right)^{1/3} r_{i,o}^{4/3} dx_{i,o}\right]^{3/4}} \tag{5.2}$$

where the subscripts i,o signify that the equation may be applied to either the inner or outer surface (see Figure 5.1). This form of equation (A1.16) is for axisymmetric flow, which is somewhat of an approximation for the cubical inner or outer body. It will be assumed, however, that this effect on overall heat transfer will be slight [33].

The heat transfer out of the inner body is

$$q = \pi k D_i^2 \frac{(T_i - \bar{T}_m)}{\bar{\Delta}_i}$$

where $\bar{T}_m$ is the as-yet undetermined average fluid temperature between the inner and outer conduction layers and D_i is the diameter of a hypothetical sphere of surface area equal to that of the inner body. Equation (5.2) may then be written as

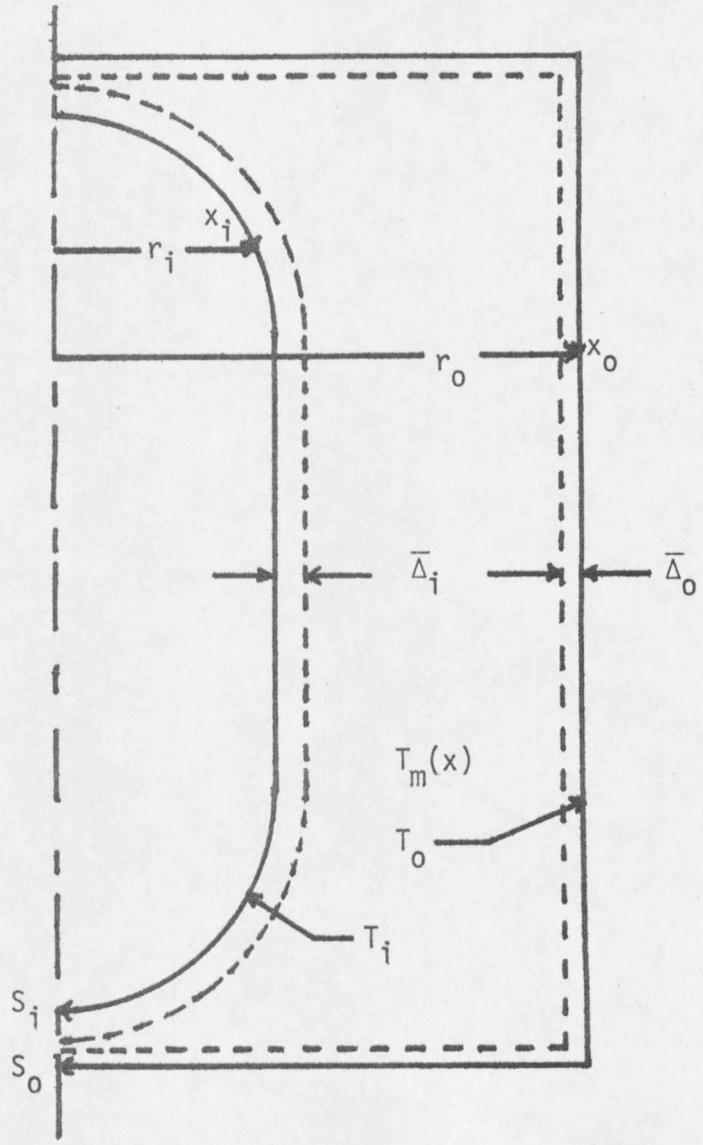


Figure 5.1 Nomenclature for the Cylinder-Cube Geometry

$$\bar{\Delta}_i = \frac{\{\frac{S_i}{D_i}\} D_i}{\bar{C}_i Ra_{D_i}^{1/4}\{(\frac{S_i}{D_i})^{3/4}\}} \frac{\{\frac{1}{S_i}\int_0^{Si} r_i\, dx_i\}}{\{[\frac{1}{S_i}\int_0^{Si}(\frac{T_i-T_m(x)}{\Delta T_r})^{5/3}(\frac{g_{x_i}}{g})^{1/3} r_i^{4/3} dx_i]^{3/4}\}} . \tag{5.3}$$

For a given shape of inner body, all terms in braces are constant and may be absorbed into $\bar{C}_i$, resulting in

$$\bar{\Delta}_i = \frac{D_i}{\bar{C}_i Ra_{D_i}^{1/4}} \tag{5.4}$$

where Ra_{D_i} is based on $T_i-\bar{T}_m$. The heat flux is then, after absorbing π into $\bar{C}_i$

$$q = kD_i(T_i-\bar{T}_m)\bar{C}_i Ra_{D_i}$$

or

$$q = kD_i\bar{C}_i[\frac{g\beta D_i^3 C_p\rho^2}{k\mu}]^{1/4}(T_i-\bar{T}_m)^{5/4} . \tag{5.5}$$

A similar analysis for the outer body leads to

$$q = kD_o\bar{C}_o[\frac{g\beta D_o^3 C_p\rho^2}{k\mu}]^{1/4}(\bar{T}_m-T_o)^{5/4} . \tag{5.6}$$

Since $\bar{T}_m$ is still undetermined, these heat fluxes may be equated under the condition on $\bar{T}_m$ such that $\bar{C}_o=\bar{C}_i=\bar{C}$, which leads to

$$q = k\bar{C}[\frac{g\beta C_p\rho^2}{k\mu}]^{1/4}\frac{(T_i-T_o)^{5/4}}{(D_i^{-7/5}+D_o^{-7/5})^{5/4}} . \tag{5.7}$$

In dimensionless form this becomes

$$Nu_\delta = \bar{C} \left\{ \frac{Ra_\delta^{1/4}}{(D_i^{-7/5} + D_o^{-7/5})^{5/4}} \frac{\delta}{\pi D_i^2}^{1/4} \right\}$$

or

$$Nu_\delta = \bar{C}_i Ra_\delta^{*1/4} \tag{5.8}$$

where δ may be any one of the three gap widths L, L', or L" discussed in Chapter IV.

Correlation (5.8) was tested against the variable density data and the results are presented in Table 5.1. The results for all data are presented in Table 5.2. Also included are results from a similar correlation:

$$Nu_\delta = C_1 Ra_\delta^{*C2} \quad . \tag{5.9}$$

Equation (5.9) correlates the data better as the Rayleigh number exponent increases above the .25 value (cf. Chapter IV). L" is the best characteristic dimension to use in equation (5.9), although no one gap width is superior in equation (5.8). It is clear that the cylinder-cube geometry is better modeled by this equivalent spheres correlation than the cube-cube geometry. This was as expected, since the cylinder used, with hemispherical end caps, is a smoothly rounded object, whereas the cube is sharp-edged and has large flat surfaces. As may be seen by comparison with Table 4.2, no improvement in the overall correlation for all geometries is effected by either equation (5.8) or (5.9).

TABLE 5.1

CORRELATIONS (5.8) AND (5.9) WITH THE VARIABLE DENSITY DATA

Equation Form	δ	Empirical Constants C_1	C_2	C_3	C_4	Average % Deviation	% of data within ±20% of equation
(5.8) all geometries	L	1.620				21.04	71.43
	L'	1.612				20.84	71.43
	L"	1.616				20.95	71.43
cylinder-cube geometry	L	1.575				18.63	70.00
	L'	1.575				18.63	70.00
	L"	1.575				18.63	70.00
cube-cube geometry	L	1.754				24.68	60.00
	L'	1.754				24.68	60.00
	L"	1.754				24.68	60.00
(5.9) all geometries	L	1.113	.308			25.28	82.86
	L'	1.109	.303			15.18	81.43
	L"	1.087	.306			14.94	84.29

TABLE 5.2

CORRELATIONS (5.8) AND (5.9) WITH ALL DATA

Equation form	δ	Empirical Constants C_1	C_2	C_3	C_4	Average % Deviation	% of data within ±20% of equation
(5.8) all geometries	L	1.840				23.13	62.24
	L'	1.846				23.28	62.24
	L"	1.850				23.40	62.24
(5.9) all geometries	L	1.268	.299			18.52	65.31
	L'	1.256	.297			18.74	66.33
	L"	1.207	.301			18.37	66.84

FLOW AROUND A CUBE

The failure of the method to correlate these geometries is that it does not account for heat transfer along horizontal surfaces, in this case on outer or inner cubes. In this section the theory will be modified to correct for horizontal flow, and a new correlation will be developed which improves the fit to the cube-cube data. This correlation will be developed for the infinite atmosphere case, which assumes that T_∞ is constant. This will lead to some error (see Appendix I), but the corresponding infinite atmosphere correlation for the cube is also presented for comparison purposes. Any error due to the infinite atmosphere approximation will then be present in both cases, and the improvement effected by the new correlation will be the difference in error between the two. In forming the infinite atmosphere correlations, T_∞ is taken as $(T_i-T_o)/2$.

The nomenclature for flow around a cube is presented in Figure 5.2. With reference to equation (A1.14), the Nusselt number may be written as

$$Nu_S = \frac{S}{\bar{\Delta}_\ell} = \frac{\bar{C}_\ell Ra_S^{1/4} \left[\frac{1}{S}\int_0^S r^{4i/3}\left(\frac{g_x}{g}\right)^{1/3} dx\right]^{3/4}}{\frac{1}{S}\int_0^S r^i\, dx} \quad . \qquad (5.10)$$

By symmetry, and assuming that the flow along each vertical cube face is independent of that along any other, the flow may be divided into four equivalent sections as shown in Figure 5.3a. Each section is thus approximately two-dimensional, so that equation (5.10) reduces to

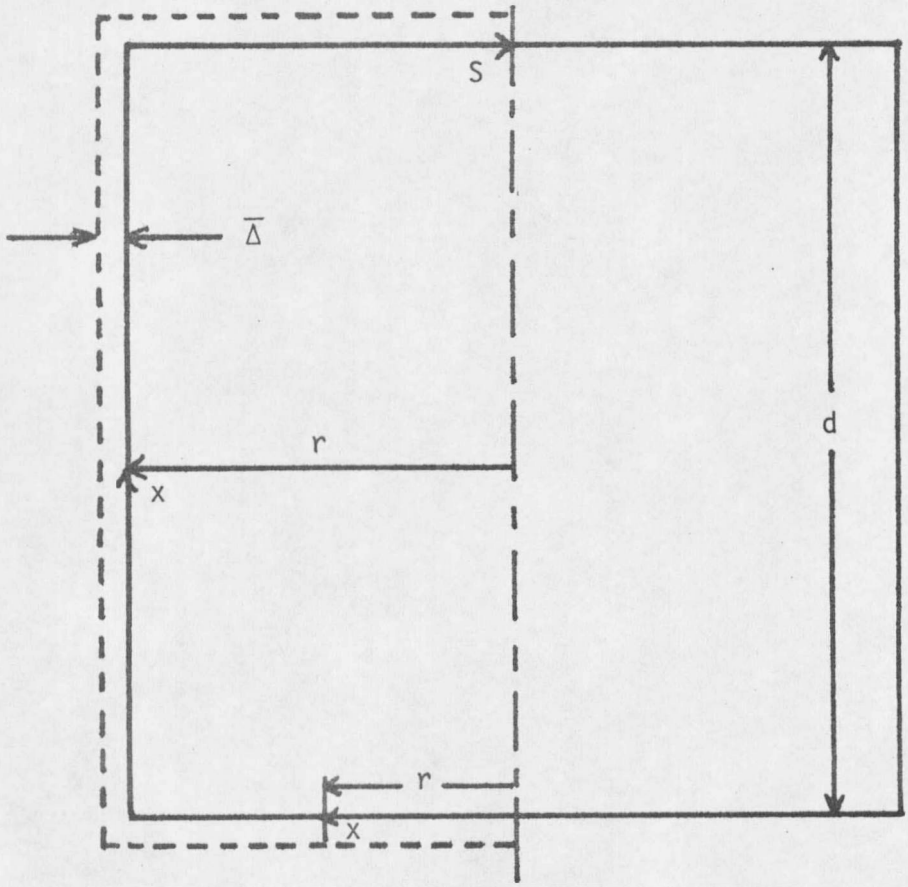


Figure 5.2 Nomenclature for Flow Around a Cube

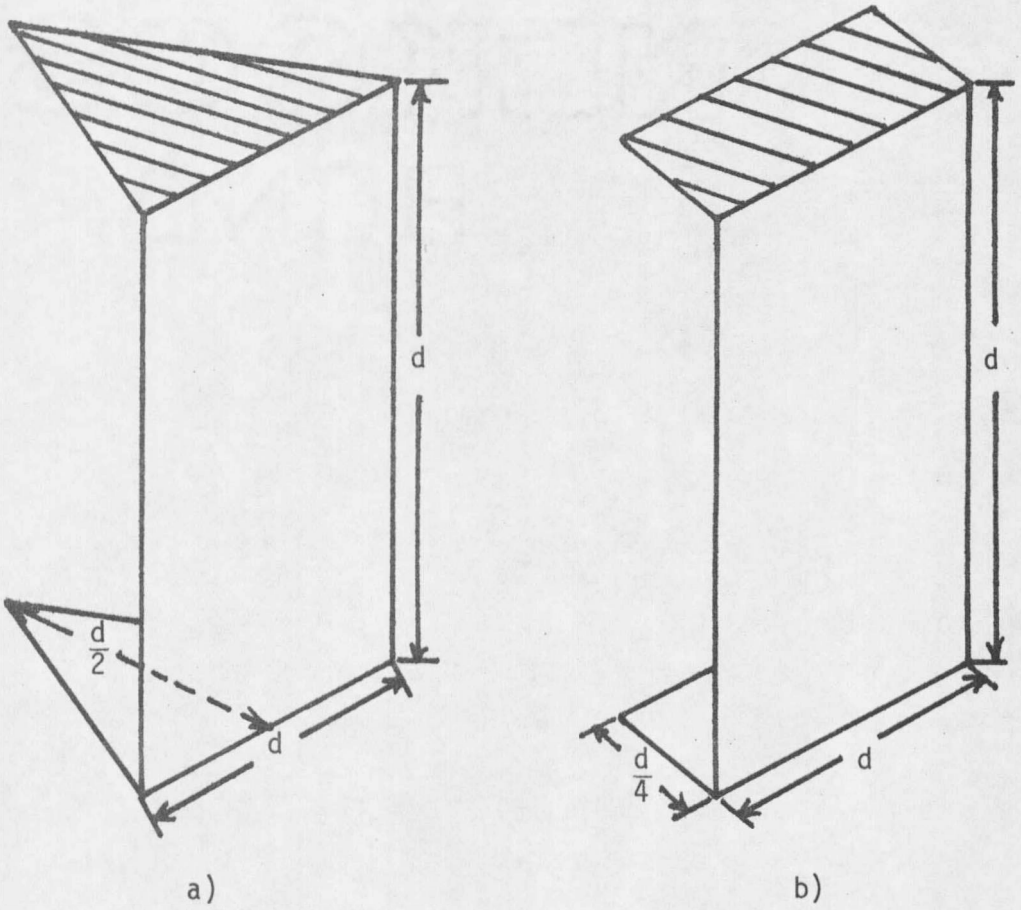


Figure 5.3 Idealization of Flow Around a Cube:
The Shaded Regions are of Equal Area

$$Nu_s = \overline{C}_\ell Ra_s^{1/4} \left[\frac{1}{S} \int_0^S \left(\frac{g_x}{g}\right)^{1/3} dx\right]^{3/4} . \qquad (5.11)$$

The integral in equation (5.11) vanishes along the top and bottom of the cube. Thus no heat transfer is predicted on these faces and the correlation reduces to the vertical plate case [4]:

$$Nu_d = .523Ra_d^{1/4} . \qquad (5.12)$$

This correlation, when applied to all of the cube-cube data, results in an average deviation of 36.13 percent, with 16.39 percent of the data falling within ±20 percent of the equation. In the correction which follows, each one fourth of the cube will be modeled as in Figure 5.3b. This involves an approximation in that the flow is modeled as strictly two-dimensional. The model is that the fluid flows uniformly over the top and bottom faces in Figure 5.3b rather than gathering towards the center of these faces as in Figure 5.3a.

Assumption #4 above does not apply along the top and bottom surfaces. It was therefore decided to form a force balance on these surfaces between viscous and acceleration, rather than buoyant, forces. Then the equation of momentum becomes

$$u \frac{\partial u}{\partial x} = \frac{\mu}{\rho} \frac{\partial^2 u}{\partial u^2} .$$

Following the suggestion of Bandrowski and Rybski [39] the velocity profile was assumed to be

$$u = u_{max}\eta(1 - \eta)^2 \qquad (5.14)$$

where $\eta=y/\delta$ (boundary layer thickness). Equation (5.14) is the velocity profile for fully developed laminar free convection between vertical plates at two different temperatures [5]. The flow between concentric cubes here is not fully developed, so the adoption of this profile does involve an approximation. δ is then replaced by Δ_ℓ, the conduction layer thickness, which introduces some further approximation (see Figure A1.1). But for fluids with Prandtl numbers not too far removed from unity, such as air, the momentum and thermal boundary layers are of comparable thickness, so that the error is probably not too great. With this assumption the velocity profile may be rewritten as

$$u = u_{max}M\frac{y}{y_m}\left(1 - M\frac{y}{y_m}\right)^2 \quad . \qquad (5.15)$$

Two final assumptions will now be made concerning the velocity profile on the top and bottom surfaces: That $du_{max}/dx=0$ and that $d\Gamma_o/dx=0$. The first of these implies that the flow is uniform and fully developed over these surfaces. This is clearly an approximation, since by symmetry the velocity grows from zero at the centers. But if the region of this growth is largely near the center, this approximation is not overly restrictive. The second approximation states that fluid enters the outer region of the boundary layer from the stagnant region at a rate which equals the growth of the inner region. The rate of growth of the inner

region is determined by a balance of energy absorbed from the wall with total energy convected in the boundary layer (see equation (5.17) below). Flow visualization data [33,40] lend some justification to this assumption in that fluid does appear to enter the boundary layer from the stagnant region as the flow advances. The physical justification of these two assumptions is tenuous at best, but the motivation for each of them is pragmatic. The first assumption leads to a much more tractable differential equation for y_m (equation (5.21) below). The second assumption alleviates the necessity of having to independently evaluate the parameter $\gamma(\overline{T}_o-T_\infty)/(T_s-T_m)$. Raithby and Hollands did not have to evaluate this parameter, because they were able to independently evaluate the parameter C_ℓ in which it appeared by means of the standard flat plate correlation (see Appendix I). But the author is aware of no such correlation for horizontal flow over horizontal surfaces, so the assumption above will be made. These two assumptions will lead to an expression for $y_m(x)$. This expression will then be modified to conform to a physically more realistic situation. The result, it is hoped, will partly compensate for unrealistic assumptions made previously.

Following the development of Appendix I, the mass flow per unit depth is obtained from an integration of u(y) from 0 to y_m:

$$\Gamma_i = \rho u_{max} M y_m \left(\frac{1}{2} - \frac{2M}{3} + \frac{M^2}{4}\right) \quad . \qquad (5.16)$$

The energy balance on the control volume in Figure A1.1 is, for $T_s > T_m$,

$$\frac{k(T_s-T_m)}{y_m} = C_p \frac{d\Gamma_i}{dx} (\overline{T}_i-T_\infty) + C_p \frac{dT_o}{dx} (\overline{T}_o-T_\infty) \quad . \qquad (5.17)$$

With the above assumption this becomes

$$\frac{k(T_s-T_m)}{y_m} = C_p \frac{d\Gamma_i}{dx} (\overline{T}_i-T_\infty) \quad . \qquad (5.18)$$

$\overline{T}_i$ is found by integration over the linear temperature profile:

$$\overline{T}_i = \frac{\int_0^{y_m} T_i u dy}{\int_0^{y_m} u \, dy}$$

which becomes

$$\frac{\overline{T}_i - T_\infty}{T_s - T_m} = B \qquad (5.19a)$$

where

$$B = \frac{1}{M} - \left[\frac{20-30M+12M^2}{30-40M+15M^2}\right] \quad . \qquad (5.12b)$$

Combining (5.18) and (5.19) yields

$$y_m \frac{d\Gamma_i}{dx} = \frac{k}{C_p B} \quad . \qquad (5.20)$$

Combining (5.20) and (5.16) results in

$$y_m \frac{d}{dx} [\rho u_{max} M y_m E] = \frac{k}{C_p B} \qquad (5.21a)$$

where

$$E = \frac{1}{2} - \frac{2M}{3} + \frac{M^2}{4} \quad . \qquad (5.21b)$$

The solution to equation (5.21) is

$$y_m = \left[\frac{2kx}{C_p u_{max}^{\rho}\ BEM}\right]^{1/2} + y_{m_o} \quad . \tag{5.22}$$

At this point the main physical hypothesis is made: that the inner region grows from zero thickness independently along each surface of the cube, so that $y_{m_o}=0$ for both the top and bottom faces. Along the vertical face, the growth of y_m is assumed to be that of the vertical flat plate case, equation (A1.9). In other words, the boundary layers are uncoupled to the extent that the inner regions are independent. The flows remain coupled in that the assumed velocity profile on the top and bottom surfaces, equation (5.14), is seen as the product of flow over the entire cube. The disturbance in the flow caused by negotiating the sharp corners of the cube is modeled as a collapse of the inner region.

Manipulation of equation (5.22) leads to the result that the inner region would grow much more quickly on the horizontal surfaces than on the vertical face, where equation (A1.9) is expected to hold. It was decided then to attenuate the growth rate of equation (5.22), but to keep the same form, so that the inner region thickness at the edge of the bottom face is the same as if it had grown along a vertical plate of the same length. To determine this attenuation factor, a specific expression is needed for u_{max}. To preserve unity, and to introduce an expression with independent physical merit, u_{max} is also chosen as the value it

would have if it had grown along the vertical plate, as with y_m, i.e., equation (A1.4) is used for u_{max}, so that

$$u_{max} = \frac{\rho\beta(T_s - T_\infty)g}{\mu} y_{ml}^2 \left[\frac{1}{2} - \frac{M}{3}\right] \tag{5.23}$$

where y_{ml} is the value described above, or for the bottom face

$$y_{ml} = \frac{ML}{C_L Ra_L^{1/4}} \tag{5.24}$$

where L=d/4. Similarly, for the top face

$$y_{ml} = \frac{M(5L)}{C_L Ra_{5L}^{1/4}} \tag{5.25}$$

When equations (5.24) and (5.23) are substituted into equation (5.22) under the described constraint, the attenuated form of equation (5.22) becomes

$$y_m = .202\left[\frac{2kx}{C_p \rho u_{max} BEM}\right]^{1/2} . \tag{5.26}$$

To perform this calculation, M was taken as Raithby and Hollands's recommended value of .4 for air.

With equation (5.26), heat fluxes can be calculated. On the bottom face, with M=.4,

$$y_m = 1.019\left[\frac{k\mu}{C_p \rho^2 \beta \Delta T g L}\right]^{1/4} x^{1/2}$$

so
$$q'' = \frac{kM(T_s - T_\infty)}{y_m}$$

and
$$q = \frac{4LkM(T_s - T_\infty)}{1.019}\left[\frac{g\beta\Delta T\rho^2 C_p L}{k\mu}\right]^{1/4}\int_0^L x^{-1/2}dx$$

$$= 7.851LkM\Delta TRa_L^{1/4} \quad . \tag{5.27}$$

Similar calculations for the top face result in

$$q = 6.421LkM\Delta TRa_L^{1/4} \quad . \tag{5.28}$$

For the vertical face, equation (A1.9) is used for y_m, so that

$$y_m = \frac{1.019x}{Ra_x^{1/4}}$$

and
$$q = \frac{4Lk\Delta TM}{1.019}\left[\frac{g\beta\Delta TC_p\rho^2}{k\mu}\right]^{1/4}\int_0^{4L} x^{-1/4}dx$$

$$= 14.818LkM\Delta TRa_L^{1/4} \quad . \tag{5.29}$$

Then the total heat transfer for this one fourth of the cube becomes

$$q = 1.028kd\Delta TRa_d^{1/4}.$$

In dimensionless form,

$$Nu_d = .868Ra_d^{1/4}. \tag{5.30}$$

Equation (5.30) correlated all of the cube-cube data with an average deviation of 16.04 percent, with 82.16 percent of the data falling within ±20 percent of the equation. The improvement gained by this analysis is

remarkable, from 36.13 to 16.04 percent average deviation. The development could most likely be improved by using more realistic assumptions about the maximum velocity and mass flow rates, and perhaps by employing a better type of constraint on the value of y_m at the bottom edge of the cube. Despite the many approximations and assumptions introduced in this development, the fit of the resulting correlation over a wide range of gap widths (Warrington's data) and pressures (the present author's data) is encouraging. It is also worth noting that this correlation was developed for the infinite atmosphere case, and still the fit is as good as any other for the cube-cube data (cf. equations (4.29)-(4.31) and Table 5.1).

CHAPTER VI

CONCLUSIONS

This investigation has demonstrated the importance of the fluid density in correlating natural convection in air at low pressures. New correlations have been generated over a wide range of air pressures. The two the author recommends most highly are

$$Nu_L = .142Ra_L^{.310}$$

$$Nu_L = .342Ra_L^{1/4} (\rho/\rho_{atm})^{.129} .$$

The density correction has been shown to be more important than the geometric correction at low pressures, as demonstrated by the good fit of the density-corrected correlations of Table 4.5. It is the author's opinion that either of the above two correlations may be used with some confidence to predict convection heat transfer in a course vacuum (pressure > 1300 Pa (10 mm Hg)) when the space surrounding the inner body is not much larger than the body itself. In infinite-atmosphere type situations, where the gap width L becomes larger than the inner body, the author recommends a boundary layer length correlation such as

$$Nu_b = .157Ra_b^{.309} .$$

It has also been shown that the characteristic dimension chosen in correlating heat transfer between three-dimensional objects is not crucial: dimensions based on gap width, bulk sizes, surface areas, or inner

body boundary layer length work equally well.

APPENDIX I

DERIVATION OF THE METHOD OF RAITHBY AND HOLLANDS

In 1975, G. D. Raithby and K. G. T. Hollands [4] published a method of generating new correlations for natural convection heat transfer. The method is based on forming a balance among buoyant, acceleration, and viscous forces in the boundary layer very close to the wall. The following is a brief outline of the physical development of the method. For greater details, the reader is invited to consult the cited publication.

It was hypothesized that the boundary layer in natural convective flow could be divided into inner and outer regions, $y \leq y_m$ and $y > y_m$ (see Figure A1.1). Under the assumption of negligible momentum transfer across the velocity extremum at y_m, the force balance in the inner region may be written independently from that in the outer region. It was further assumed that acceleration forces in the inner region are negligible. Other assumptions included: all fluid properties are constant; boundary layers are very small relative to the radius of curvature of the submerged body; the temperature protile in the inner region is linear (Figure A1.1); the ratio of the buoyant force in the inner region to the total buoyancy of the boundary layer is a function of the Prandtl number only and invariant with x, the position along the body.

The momentum equation in the x direction is

$$\frac{\partial^2 u}{\partial x^2} = \frac{\rho_\infty - \rho(y)}{\mu} g_x \qquad \text{(A1.1)}$$

where g_x is the gravitational acceleration in the direction of x. With

the linear temperature profile assumption and the approximation

$$\rho_\infty - \rho = \rho\beta(T - T_\infty)$$

one may write

$$\rho_\infty - \rho(y) = -\rho\beta(T_\infty - T_S)(1 - M\frac{y}{y_m}) \qquad (A1.2)$$

where

$$M = \frac{T_M - T_S}{T_\infty - T_S} = \frac{y_m}{\Delta_\ell} .$$

Δ_ℓ is the local thickness of a stagnant conduction layer with heat transfer equivalent to the actual convection heat transfer. Substituting (A1.2) into (A1.1), one obtains

$$\frac{\partial^2 u}{\partial y^2} = -\rho\beta\frac{(T_\infty - T_x)}{\mu} g_x(1 - \frac{M}{y_m} y) . \qquad (A1.3)$$

Integrating this equation with appropriate boundary conditions at y=0 and $y=y_m$ yields

$$u = \frac{\rho\beta(T_\infty - T_S)}{\mu} g_x \{(yy_m - y^2/2) - M(\frac{yy_m}{2} - \frac{y^3}{6y_m})\} . \qquad (A1.4)$$

Equation (A1.4) is then integrated to give the mass flow per unit depth (into the paper in Figure A1.1):

$$\Gamma_i = \rho^2\beta\frac{(T_\infty - T_S)}{\mu} g_x(\frac{y_m^3}{3})(1 - \frac{5M}{8}) . \qquad (A1.5)$$

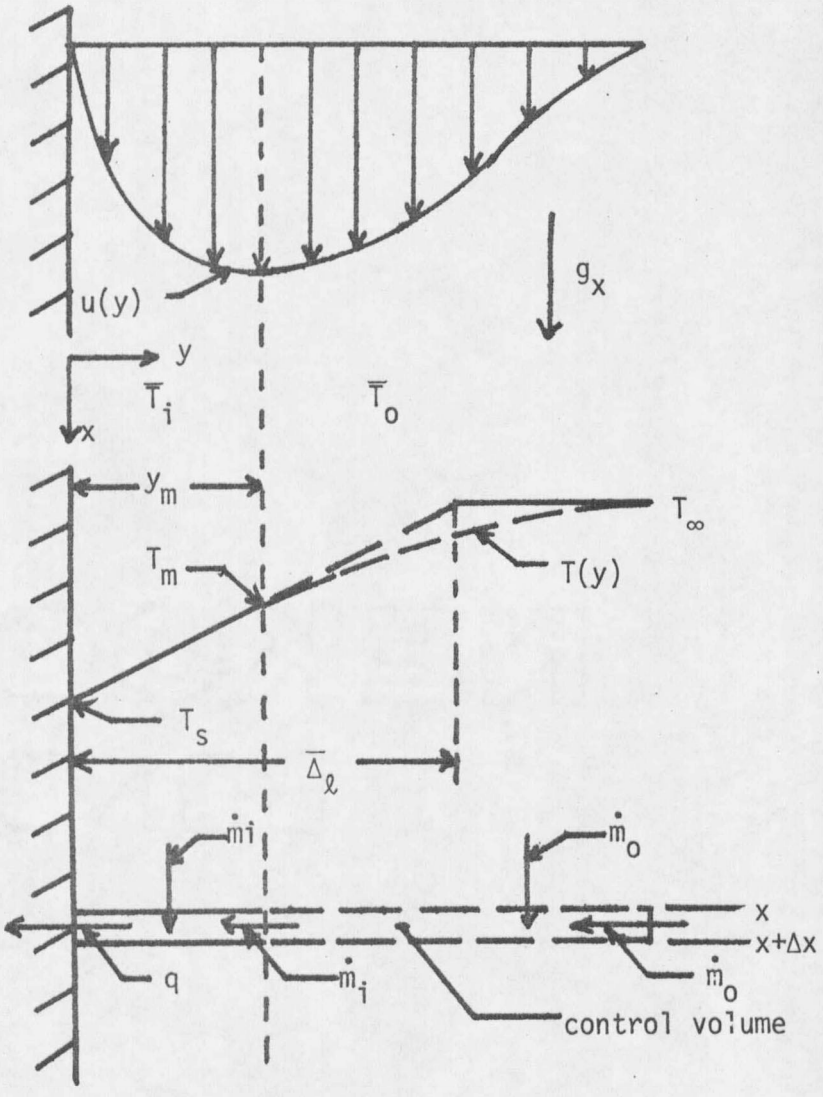


Figure A1.1 Nomenclature of the Method of Raithby and Hollands

The energy balance for the control volume in Figure A1.1 is

$$k \frac{(T_M - T_S)}{y_m} = \frac{d\Gamma_i}{dx} Cp(T_\infty - \overline{T}_i) + \gamma \frac{d\Gamma_i}{dx} Cp(T_\infty - \overline{T}_o) \qquad (A1.6)$$

where the definitions

$$\gamma = \frac{d\Gamma_o/dx}{d\Gamma_i/dx}$$

and $\overline{T}_{i,o}$ = average inner, outer fluid temperature

have been used. $\overline{T}_i$ is found by using the linear temperature profile assumption and equation (A1.4):

$$\overline{T}_i = \frac{\int_0^{y_m} T_i \, u \, dy}{\int_0^{y_m} u \, dy} \quad , \text{ which becomes}$$

$$\overline{T}_i = T_s + (T_m - T_s) \frac{5/8 - 2M/5}{1 - 5M/8} \; .$$

This may be rewritten as

$$\frac{T_\infty - \overline{T}_i}{T_M - T_S} = \frac{1}{M} - \frac{5/8 - 2M/5}{1 - 5M/8} \; . \qquad (A1.7)$$

Equations (A1.5) and (A1.7) are combined to yield

$$y_m \frac{d\Gamma_i}{dx} = k/\{Cp[\frac{1}{M} - \frac{5/8 - 2M/5}{1 - 5M/8} + \gamma \frac{T_\infty - \overline{T}_o}{T_M - T_S}]\} \; . \qquad (A1.8)$$

Equations (A1.5) and (A1.8) could be solved for y_m, and thus for the heat

transfer, if the parameters M and $\gamma(T_\infty-\overline{T}_o)/(T_m-T_s)$ were known. At this point the main hypothesis of the development was advanced: that these two parameters depend only on the Prandtl number (Pr) of the fluid and not on the geometry, as long as the condition $y_m<<R(x)$ (radius of curvature) is fulfilled. With this hypothesis, the Pr dependence of these parameters may be found for any geometry and then applied to any other geometry.

The authors found the Pr dependence for the case of the vertical flat plate. Specifically, the Pr dependence of a new single parameter in which only the above two parameters appear was determined. The analysis begins by combining equations (A1.5) and (A1.8), realizing that $g_x=g=$constant for this case, to obtain after integration

$$y_m = \frac{Mx}{C_\ell Ra_x^{1/4}} \tag{A1.9}$$

where

$$C_\ell = M\left[\frac{1-5M/8}{12}\left\{\frac{1}{M} - \frac{5/8-2M/5}{1-5M/8} + \gamma\frac{T_\infty-\overline{T}_o}{T_\infty-T_m}\left(\frac{1}{M}-1\right)\right\}\right]^{1/4} \tag{A1.10}$$

and Ra_x is based on $T_\infty-T_s$. The importance of C_ℓ may be demonstrated by first formulating the heat flux into the wall

$$\frac{q}{A} = k\frac{(T_m-T_s)}{y_m}$$

and thus the local heat transfer coefficient

$$h_x = \frac{q_x}{A(T_\infty - T_s)} = \frac{k}{y_m}\frac{T_m - T_s}{T_\infty - T_s} = \frac{kM}{y_m} \quad .$$

The heat transfer correlation then becomes

$$Nu_x = \frac{h_x X}{k} = \frac{xM}{y_m} = C_\ell Ra_x^{1/4} \quad .$$

The heat transfer may thus be calculated when the Pr dependence of C_ℓ alone is known. No knowledge of the Pr dependence of the two parameters M and $\gamma(T_\infty - \overline{T}_o)/(T_m - T_s)$ is required. The authors quoted a similar solution result of Rohsenow and Choi [38] for C_ℓ:

$$C_\ell = 0.48[Pr/(.861+Pr)]^{1/4}$$

which was then used to replace equation (A1.10) in the general case.

In extending the method to two-dimensional and axisymmetric geometries, the authors first defined an equivalent conduction thickness

$$\Delta_\ell(x) = \frac{k}{h_x} \quad , \quad \text{or} \quad Nu_x = \frac{X}{\Delta_\ell(x)} \quad .$$

In steps which resemble the vertical flat plate development, an equation for Γ_i is found by eliminating y_m from (A1.8) using (A1.5):

$$\frac{d\Gamma_i^{4/3}}{dx} = \frac{4k}{3BCp}\left[\frac{\rho^2 g_x \beta(T_\infty - T_s)}{3\mu}\left(1-\frac{5M}{8}\right)\right]^{1/3} \qquad (A1.11)$$

where

$$B = \frac{1}{M} - \frac{5/8-2M/5}{1-5M/8} + \gamma \frac{T_\infty - \bar{T}_o}{T_m - T_s} \qquad (A1.12)$$

Solution of this differential equation with the boundary condition $\Gamma_i=0$ at x=0 (see Figure A1.2) yields

$$\Delta_\ell(x) = \frac{x}{C_\ell Ra_x^{1/4}} \frac{\left[\frac{1}{x}\int_o^x \left(r^{4i}\frac{g_x}{g}\right)^{1/3} dx\right]^{1/4}}{\left(r^i \frac{g_x}{g}\right)^{1/3}} . \qquad (A1.13)$$

The average conduction thickness is found by an integration of the local heat transfer over the length of the boundary layer, resulting in

$$\bar{\Delta}_\ell = \frac{S}{\bar{C}_\ell Ra_S^{1/4}} \frac{\frac{1}{s}\int_o^s r^i\, dx}{\left[\frac{1}{s}\int_o^s \left(r^{4i}\frac{g_x}{g_x}\right)^{1/3} dx\right]^{3/4}} . \qquad (A1.14)$$

In these equations, i=0 and i=1 for two-dimensional and axisymmetric geometries, respectively, and $\bar{C}_\ell=(4/3)C_\ell$.

The final modification of the theory for application to convection within enclosures involves the fact that T_∞ is no longer constant with x. In this case the energy equation (A1.6) becomes

$$k\left(\frac{T_m-T_s}{y_m}\right) = Cp\frac{d}{dx}\left[\Gamma_i(T_\infty-\bar{T}_i)\right] + Cp\frac{d}{dx}\left[\Gamma_o(T_\infty-\bar{T}_o)\right].$$

The assumption that B, equation (A1.12), depends only on Pr is somewhat less satisfactory here because of possible variation as $T_\infty-T_S$ changes.

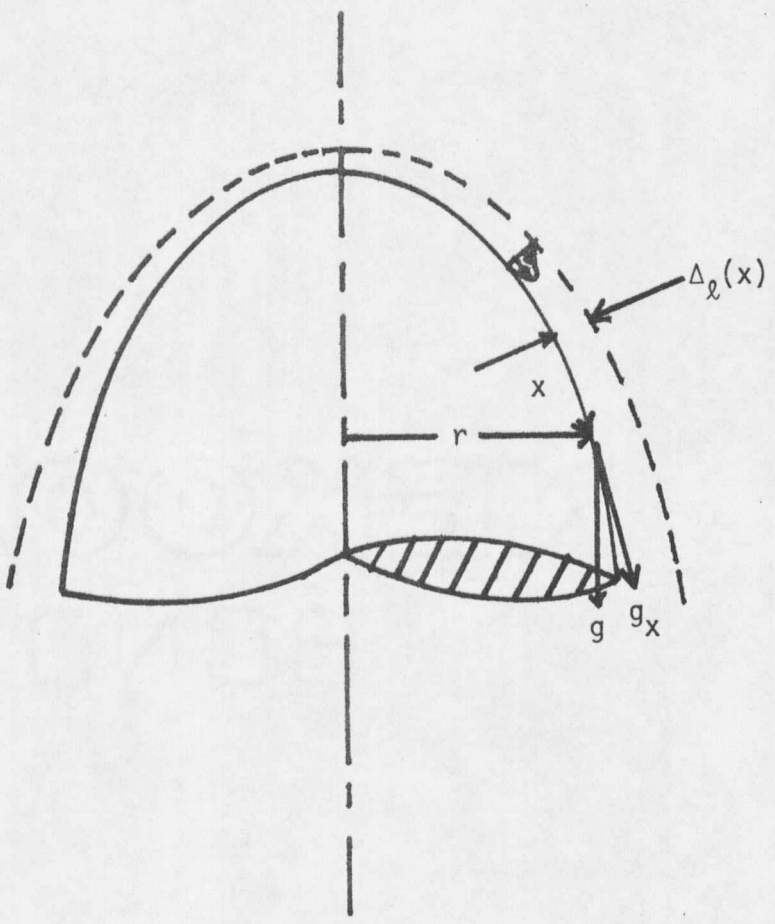


Figure A1.2 Nomenclature for Two-Dimensional or Axisymmetric Flow

Realizing this approximation and proceeding as before yields

$$\Delta_\ell(x) = \frac{x}{C_\ell Ra_x^{1/4}} \frac{\left[\frac{1}{x\Delta T^{4/3}} \int_0^x \left(r^{4i} \frac{g_x}{g} \frac{\Delta T}{\Delta T_r}\right)^{1/3} \Delta T^{4/3}\, dx\right]^{1/4}}{\left(r^i \frac{g_x}{g} \frac{\Delta T}{\Delta T_r}\right)^{1/3}} \qquad \text{(A1.15)}$$

where ΔT_r is some reference temperature difference on which Ra_x is based. The average conduction thickness becomes

$$\bar{\Delta}_\ell = \frac{S}{\bar{C}_\ell Ra_s^{1/4}} \frac{\frac{1}{s}\int_0^s r^i\, dx}{\left[\frac{1}{s}\int_0^s \left(\frac{\Delta T}{\Delta T_r}\right)^{5/3} \left(\frac{g_r}{g}\right)^{1/3} r^{4i/3}\, dx\right]^{3/4}} . \qquad \text{(A1.16)}$$

Equations (A1.13-A1.16) are then the starting point for the analysis in Chapter V.

APPENDIX II

DATA REDUCTION PROGRAMS

The following are Fortran IV programs used to reduce the heat transfer and temperature profile data. The subroutines CURFT and ERROR are used to correlate the heat transfer and are called when needed by the mainline program. The function T is used to convert thermocouple readings to temperatures. The inputs to the heat transfer program are the dimensions of the inner and outer bodies, their temperatures, the convection heat transfer rate, and the pressure. The inputs to the temperature profile program are the local gap width, the temperatures of the inner and outer bodies, and the micrometer and thermocouple readings at each step in the traverse.

```
      DIMENSION GHOPE(500),RASTAR(500),XXNUS(500),X(6,500)
      DIMENSION ZASTAR(500),GEO(500),XPR(500),
     1   ZZNUS(500),XRA(500),ZRA(500),C(6),DEN1(500)
C
C***HEAT TRANSFER DATA REDUCTION
C
C***K IS A COUNTER
      K=0
      PI=3.1415927
C***READ IN A NEGATIVE VALUE OR ZERO FOR IDB FOR LAST RUN
   50 READ (105,25) IDB,XCUBE,SD,XXX,TAVGI,TAVGO,P,PRESMM
   25 FORMAT (I5,7F9.4)
C***IDB IS THE GEOMETRY IDENTIFIER
C       1-SPHERICAL INNER BODIES
C       2-CYLINDRICAL INNER BODIES
C       3-CUBICAL INNER BODIES
C***XXX IS A RATIO OF CYLINDER AND OUTER BODY DIMENSIONS
C       XXX=(LENGTH OVERALL-SD)/(XCUBE-SD)
C***XCUBE, SD, AND XLEN ARE OUTER AND INNER BODY DIMENSIONS
C***P IS THE CONVECTION HEAT TRANSFER (BTU/HR)
C***PRESMM IS THE EXPERIMENTAL AIR PRESSURE (MM HG)
C***SA IS THE INNER BODY SURFACE AREA
C***RI IS THE RADIUS OF AN EQUIVALENT VOLUME INNER SPHERE
C***DI IS THE RADIUS OF AN EQUIVALENT AREA INNER SPHERE
C***RO AND DO ARE CORRESPONDING VALUES FOR THE OUTER BODY
C***BLL IS THE LENGTH OF THE BOUNDARY LAYER ON THE INNER BODY
C***ALL DIMENSIONS ARE IN INCHES
C
      IF (IDB) 100,100,30
   30 K=K+1
      IF (K.EQ.1) OUTPUT IDB,SD,XXX
      GO TO (4,5,6) IDB
C***SPHERES, CUBICAL OUTER BODY
    4 SA=PI*SD*SD
      RO=((3.*XCUBE**3)/(4.*PI))**(1./3.)
      RI=SD/2.
      GAP=RO-SD/2.
      IF (SD.EQ.4.5) GRATIO=.9176;GAP1=4.47
      IF (SD.EQ.7.0) GRATIO=.801362;GAP1=3.22
      IF (SD.EQ.9.0) GRATIO=.582401;GAP1=2.22
      BLL=PI*SD/2.
      DI=SD
      GO TO 11
```

```
C***CYLINDERS,CUBICAL OUTER BODY
     5 XLEN=XXX*(XCUBE-SD)+SD
       SA=PI*SD*(XLEN-SD)+PI*SD*SD
       RO=((3.*XCUBE**3)/(4.*PI))**(1./3.)
       RI=(SD/4.)*((12.*XLEN/SD)-4.)**(1./3.)
       GAP=RO-RI
       IF (XXX.EQ.0.3083) QRATIO=1.2289;GAP1=4.58
       IF (XXX.EQ.0.5429) QRATIO=1.1243;GAP1=3.49
       IF (XXX.EQ.0.3143) QRATIO=.9691;GAP1=3.31
       IF (XXX.EQ.0.7333) QRATIO=1.8200;GAP1=4.083
       BLL=PI*SD/2.+XLEN-SD
       DI=SQRT(SD*XLEN)
       GO TO 11
C***CUBES,CUBICAL OUTER BODY
     6 SA=6.*SD*SD
       RO=((3.*XCUBE**3)/(4.*PI))**(1./3.)
       RI=((3.*SD**3)/(4.*PI))**(1./3.)
       GAP=RO-RI
       IF (SD.EQ.4.0) QRATIO=1.4709;GAP1=4.16
       IF (SD.EQ.5.0) QRATIO=1.5235;GAP1=3.53
       IF (SD.EQ.6.4) QRATIO=1.6278;GAP1=2.63
       BLL=SD*2.
       DI=SQRT(SA/PI)
    11 CONTINUE
       DO=14.510
       GAP2=(DO-DI)/2.
C***DT IS TEMP DIFFERENCE BETWEEN INNER & OUTER BODIES
       DT=TAVGI-TAVGO
C***H IS THE AVERAGE HEAT TRANSFER COEFFICIENT (B/HR-FT**2-F)
       H=P*144./(DT*SA)
C***CALCULATE THE MEAN TEMPERATURE (DEG F)
       TM=(TAVGI+TAVGO)/2.
C***TAVG, MEAN TEMPERATURE (DEG R)
       TAVG=TM+459.69
C***CALCULATE THE FLUID PROPERTIES
C***ABSOLUTE VISCOSITY OF AIR (LBM/HR-FT)
       C0=134.375
       C1=6.0133834
       C2=1.8432899
       C3=1.3347050
       VIS=TAVG**C2/(EXP(C1)*(TAVG+C0)**C3)
C***SPECIFIC HEAT OF AIR (BTU/LBM-R)
       C0=2.236775/(10.**5)
       C1=.28797749
       SH=C1+C0*TAVG
```

```
C***THERMAL CONDUCTIVITY OF  AIR (BTU/HR-FT-F)
      XP=.1
      C0=-8.5964965
      C1=34490.89
      C2=868.23837
      C3=8056583.8
    7 FX=XP
      F=C0+C1*FX+C2*FX*FX+C3*FX*FX*FX-TAVG
      FP=C1+2.*C2*FX+3.*FX*FX*C3
      XP=FX-F/FP
      IF (ABS((XP-FX)/FX)-.0001) 8,8,7
    8 COND=XP
C***DENSITY OF AIR (LBM/FT**3)
      DEN=.07625*(PRESMM/760.)*(519.69/TAVG)
      DEN1(K)=DEN
C*THERMAL EXPANSION COEFFICIENT OF AIR (1/R)
      BET=1./TAVG
C***THE PRANDTL NUMBER
      PR=VIS*SH/COND
      XPR(K)=PR
C***THE GRASHOF NUMBER
      GR=32.174*BET*DT*(GAP**3./1728.)*DEN*DEN*3600.*3600./(VIS*VIS)
C***THE NUSSELT NUMBER
      XXNUS(K)=H*GAP/(COND*12.)
C***THE RAYLEIGH NUMBER
      RA=GR*PR
      XRA(K)=RA
      GEO1=GAP**.25/)(DI**(-1.4)+DO**(-1.4))**1.25*PI*DI*DI)
C***RASTAR IS THE MODIFIED RAYLEIGH NUMBER (RA*GAP/RI)
      RASTAR(K)=RA*GAP/RI
C***QSPH IS THE HEAT TRANSFER BY CONDUCTION BETWEEN CONCENTRIC SPHERES
      QSPH=PI*COND*XCUBE*SD*DT/(6.*(XCUBE-SD))
      QCOND=QRATIO*QSPH
C***QHOPE IS THE RATIO OF Q CONVECTION TO Q CONDUCTION
      QHOPE(K)=P/QCOND
      GEO(K)=GAP/RI
C***CALCULATE PARAMETERS BASED ON THE BOUNDARY LAYER LENGTH
      GR=32.174*BET*DT*(BLL*BLL*BLL/1728.)*DEN*DEN*3600.*3600./(VIS*VIS)
      XNUS=H*BLL/(COND*12.)
      RA=GR*PR
      ZRA(K)=RA
      ZASTAR(K)=RA*GAP/RI
      ZZNUS(K)=XNUS
      GO TO 50
  100 CONTINUE
```

```
C***OUTPUT DIMENSIONLESS RESULTS
      WRITE (108,2000)
 2000 FORMAT (1H1,7HRUN NO.,3X,17HGEOMETRIC FACTORS)
      WRITE (108,2001)
 2001 FORMAT (1H ,10X,15H  QHOPE      GEO)
      DO 200 NN=1,K
      Q=QHOPE(NN)
      G=GEO(NN)
      WRITE (108,2002) NN,Q,G
 2002 FORMAT (1H ,I5,E14.4,E11.4)
  200 CONTINUE
      WRITE (108,3000)
 3000 FORMAT (1H0,7HRUN NO.,11X,17HGAP WIDTH RESULTS,
     1    15X,29HBOUNDARY LAYER LENGTH RESULTS)
      WRITE (108,3001)
 3001 FORMAT (1H ,14X,3HNUS,8X,2HRA,7X,6HRASTAR,12X,
     1    3HNUS,8X,2HRA,7X,6HRASTAR)
      DO 300 NN=1,K
      XNUS=XXNUS(NN)
      RAX=XRA(NN)
      RASTX=RASTAR(NN)
      ZNUS=ZZNUS(NN)
      RAZ=ZRA(NN)
      RASTZ=ZASTAR(NN)
      WRITE (108,3002) NN,XNUS,RAX,RASTX,ZNUS,RAZ,RASTZ
 3002 FORMAT (1H ,I5,E16.4,2E11.4,E16.4,2E11.4)
  300 CONTINUE
C***THE FOLLOWING STEPS ARE DIFFERENT FOR
C          DIFFERENT CORRELATIONS
      DO 115 N=1,K
      X(1,N)=1.
      X(2,N)=ALOG10(XRA(N))
  115 X(3,N)=ALOG10(XXNUS(N))
      NV=2;NOB=K
      OUTPUT 'CORRELATION #1'
      CALL CURFT(NV,NOB,X,C)
      CALL ERROR(NV,NOB,X,C,SSQ)
      C1=10.**C(1);OUTPUT C1
      END
```

```
      SUBROUTINE CURFT(NV,NOB,X,C)
       DIMENSION X(6,250),C(6),S(7,7)
      DOUBLE PRECISION S,D
C     LEAST SQUARES - NV INDEPENDENT VARIABLES
C          WRITTEN BY R. E. POWE - MECHANICAL ENGINEERING
C     Y=X(NV+1,I) - NOB= NO. OF OBSERVATIONS
C     C(I)=COEFFICIENT OF X(I)
      M=NV+1
      MP=M+1
      DO 1 I=1,M
      DO 1 J=1,MP
    1 S(I,J)=0.D0
      DO 2 I=1,NOB
      DO 2 J=1,M
      DO 2 K=1,M
    2 S(J,K)=S(J,K)+X(J,I)*X(K,I)
      S(1,MP)=1.D0
      IF (NV-1) 997,997,998
  997 S(1,1)=S(1,2)/S(1,1)
      GO TO 999
  998 DO 16 LK=1,NV
   11 IF (S(1,1)) 13,12,13
   12 WRITE (108,20)
   20 FORMAT (' EQUATIONS IN SUBROUTINE CURFT ARE DEPENDENT - IGNORE FOL
     1LOWING ERROR ANALYSIS')
      DO 30 III=1,NV
   30 C(III)=0.
      GO TO 31
   13 DO 14 J=1,M
   14 S(M,J)=S(1,J+1)/S(1,1)
      DO 15 I=2,NV
      D=S(I,1)
      DO 15 J=1,M
   15 S(I-1,J)=S(I,J+1)-D*S(M,J)
      DO 16 J=1,M
   16 S(NV,J)=S(M,J)
  999 DO 3 I=1,NV
      C(I)=S(I,1)
    3 WRITE (108,4) I,C(I)
    4 FORMAT (' ',10X,'COEFFICIENT OF X',I2,'=',E15.8)
   31 RETURN
      END
```

```
      SUBROUTINE ERROR(NV,NOB,X,C,SSQ)
      DIMENSION X(6,400),C(6),S(10,10),ANP(10),RNRL(400),RNRLS(400)
      DOUBLE PRECISION YC,TS,TE,YC1
C     ERROR ANALYSIS - NOB OBSERVATIONS
C     Y=X(NV+1,I) - SSQ=STANDARD DEVIATION
C     C(I) - CONSTANTS
C        WRITTEN BY R. E. POWE - MECHANICAL ENGINEERING
      M=NV+1
      TS=0.D0
      TE=0.D0
      EMX=0.
      DO 5 I=1,5
    5 ANP(I)=0.
      WRITE (108,1)
    1 FORMAT ('0',5X,'Y EXPERIMENTAL',8X,' Y CALCULATED',5X,
     1   'NUMERICAL ERROR',5X,'PER CENT ERROR')
      DO 2 I=1,NOB
      YE=X(M,I)
C     ADD EQUATION FOR YC AT THIS POINT
      YC=0.D0
      YC=C(1)+C(2)*X(2,I)
      YC1=10.**YC
      YE1=10.**YE
      E=YC1-YE1
      EP=100.*E/YE1
      EPA=ABS(EP)
      IF (EPA-EMX) 6,6,7
    7 EMX=EPA
    6 DO 8 J=1,5
      ACD=J*5
      IF (EPA-ACD) 9,9,8
    9 ANP(J)=ANP(J)+1.
    8 CONTINUE
      TS=TS+E*E
      TE=TE+ABS(EP)
    2 WRITE (108,3) YE1,YC1,E,EP,I
    3 FORMAT (4E20.8,I5)
      A=NOB
      SSQ=(TS/A)**.5
      TE=TE/A
      WRITE (108,4) SSQ,TE
    4 FORMAT ('0',10X,'STANDARD DEVIATION=',E15.8,5X,'AVERAGE PER CENT D
     1EVIATION=',E15.8)
      WRITE (108,10) EMX
   10 FORMAT ('0',30X,'MAXIMUM PER CENT DEVIATION=',E15.8)
```

```
      DO 11 I=1,5
      XNP=ANP(I)
      XNP=100.*XNP/A
      ACD=I*5
   11 WRITE (108,12) XNP,ACD
   12 FORMAT (5X,E15.8,2X,'PER CENT OF DATA WITHIN',2X,E15.8,2X,
     1    'PER CENT  OF EQUATION')
      RETURN
      END
```

```
C***TEMPERATURE PROFILE MAINLINE
      K=0
   20 K=K+1
C***DR IS GAP SPACING
C***VHIGH&VLOW ARE THERMOCOUPLE READINGS AT ENDS OF TRAVERSE
      READ (105,2000) DR,VHIGH,VLOW
 2000 FORMAT (3F10.4)
C***READ IN A NEGATIVE OR ZERO FOR DR FOR LAST PROFILE
      IF (DR) 100,100,30
   30 GO TO (31,32,34,36) K
   31 WRITE (108,4001)
 4001 FORMAT (1H1,'PROBE NO. 1')
      GO TO 40
   32 WRITE (108, 4002)
 4002 FORMAT (1H1,'PROBE NO.2')
      GO TO 40
   34 WRITE (108,4004)
 4004 FORMAT (1H1,'PROBE NO. 4')
      GO TO 40
   36 WRITE (108,4006)
 4006 FORMAT (1H1,'PROBE NO. 6')
   40 THIGH=T(VHIGH)
      TLOW=T(VLOW)
      DT=THIGH-TLOW
      WRITE (108,3000)
 3000 FORMAT (1H0,'DIMENSIONLESS DISTANCE     DIMENSIONLESS TEMPERATURE'
)
C***READ IN MICROMETER AND THERMOCOUPLE READINGS
   45 READ (105,2001) FMICRO,VOLT
 2001 FORMAT (2F10.4)
C***READ IN A NEGATIVE OR ZERO FOR VOLT FOR LAST READING IN PROFILE
      IF (VOLT) 20,20,50
   50 RSTAR=(DR-FMICRO)/DR
      TT=T(VOLT)
      TSTAR=(TT-TLOW)/DT
      WRITE (108,3001) RSTAR,TSTAR
 3001 FORMAT (1H ,F16.4,F28.4)8
      GO TO 45
  100 CONTINUE
      END
```

```
      FUNCTION T(E)
      DIMENSION C(8)
      DOUBLE PRECISION TOT
      C(1)=491.96562
      C(2)=46.381884
      C(3)=-1.3918864
      C(4)=0.15260798
      C(5)=-0.020201612
      C(6)=0.0016456956
      C(7)=-6.6287090/(10.**5)
      C(8)=1.0241343/(10.**6)
      TOT=0.D0
      DO 1 I=1,8
    1 TOT=TOT+C(I)*(E**(I-1))
      T=TOT
      RETURN
      END
```

APPENDIX III

PARTIALLY REDUCED DATA

The following is a listing of all the data used in the heat transfer program, including that of Warrington [33]. The data were reduced to this form on a Texas Instruments SR-40 calculator. The dimensions are inches on XCUBE and SD, °F on TAVGI and TAVGO, BTU/hr on P, and mm Hg on PRESMM. IDB and XXX are unitless.

IDB	XCUBE	SD	XXX	TAVGI	TAVGO	P	PRESMM
2	10.5000	4.5000	.7333	99.804	50.954	2.846	19.4
2	10.5000	4.5000	.7333	130.174	50.470	5.962	19.4
2	10.5000	4.5000	.7333	125.619	49.152	9.081	48.0
2	10.5000	4.5000	.7333	103.574	48.181	4.276	48.0
2	10.5000	4.5000	.7333	82.299	47.192	3.663	48.0
2	10.5000	4.5000	.7333	69.402	48.509	1.982	48.0
2	10.5000	4.5000	.7333	68.596	45.568	3.321	99.9
2	10.5000	4.5000	.7333	81.703	46.545	5.291	99.9
2	10.5000	4.5000	.7333	95.094	46.727	6.015	99.9
2	10.5000	4.5000	.7333	121.952	49.500	13.001	99.9
2	10.5000	4.5000	.7333	119.798	47.649	16.184	145.5
2	10.5000	4.5000	.7333	99.920	48.030	9.457	145.5
2	10.5000	4.5000	.7333	83.612	50.052	6.162	149.6
2	10.5000	4.5000	.7333	75.386	49.431	3.662	145.5
2	10.5000	4.5000	.7333	70.929	45.621	4.764	199.7
2	10.5000	4.5000	.7333	83.510	46.212	7.959	199.7
2	10.5000	4.5000	.7333	106.169	49.210	14.024	199.7
2	10.5000	4.5000	.7333	132.035	51.061	24.398	199.7
2	10.5000	4.5000	.7333	128.958	49.444	25.624	248.8
2	10.5000	4.5000	.7333	108.507	49.319	16.389	248.8
2	10.5000	4.5000	.7333	92.225	49.440	10.536	248.8
2	10.5000	4.5000	.7333	73.122	48.098	4.156	248.8
2	10.5000	4.5000	.7333	74.966	50.871	7.298	303.0
2	10.5000	4.5000	.7333	91.109	49.268	12.563	303.0
2	10.5000	4.5000	.7333	106.382	48.750	18.613	304.1
2	10.5000	4.5000	.7333	129.896	51.834	29.382	305.8
2	10.5000	4.5000	.7333	125.856	50.149	32.018	396.8
2	10.5000	4.5000	.7333	107.952	46.098	23.089	396.8
2	10.5000	4.5000	.7333	87.826	46.667	13.198	396.8
2	10.5000	4.5000	.7333	69.886	47.270	7.541	396.8
2	10.5000	4.5000	.7333	73.158	51.083	8.429	505.7
2	10.5000	4.5000	.7333	92.087	50.773	16.991	505.7
2	10.5000	4.5000	.7333	110.038	49.327	27.738	505.7
2	10.5000	4.5000	.7333	125.850	46.917	39.503	505.7
2	10.5000	4.5000	.7333	124.660	45.750	44.022	599.7
2	10.5000	4.5000	.7333	112.045	51.174	30.895	599.7
2	10.5000	4.5000	.7333	92.587	48.166	19.270	599.7
2	10.5000	4.5000	.7333	73.686	47.991	11.095	599.7
2	10.5000	4.5000	.7333	4.270	48.046	11.653	641.9
2	10.5000	4.5000	.7333	89.558	52.341	16.895	641.9
2	10.5000	4.5000	.7333	109.518	48.312	32.653	641.9
2	10.5000	4.5000	.7333	127.956	49.575	45.272	641.9
2	10.5000	4.5000	.7333	106.912	49.025	4.037	29.9
2	10.5000	4.5000	.7333	96.926	50.014	2.816	29.9
2	10.5000	4.5000	.7333	122.590	53.667	3.087	15.9

2	10.5000	4.5000	.7333	125.194	52.136	3.967	16.1
2	10.5000	4.5000	.7333	102.604	54.310	6.044	74.0
2	10.5000	4.5000	.7333	87.174	52.568	3.827	74.0
2	10.5000	4.5000	.7333	79.606	52.409	3.051	74.0
2	10.5000	4.5000	.7333	124.833	52.477	11.826	74.0
3	10.5000	5.0000	.0000	110.203	49.613	2.289	17.4
3	10.5000	5.0000	.0000	135.444	47.099	11.561	38.1
3	10.5000	5.0000	.0000	113.310	48.258	5.390	39.2
3	10.5000	5.0000	.0000	62.213	45.560	4.354	39.8
3	10.5000	5.0000	.0000	66.181	45.265	3.940	93.4
3	10.5000	5.0000	.0000	102.986	46.682	10.715	95.6
3	10.5000	5.0000	.0000	166.880	48.546	38.782	100.9
3	10.5000	5.0000	.0000	116.551	50.424	13.018	97.9
3	10.5000	5.0000	.0000	72.412	48.144	6.288	186.1
3	10.5000	5.0000	.0000	88.471	47.697	10.461	197.3
3	10.5000	5.0000	.0000	136.972	48.717	34.688	201.0
3	10.5000	5.0000	.0000	121.556	50.673	30.231	297.4
3	10.5000	5.0000	.0000	80.523	46.311	11.374	297.4
3	10.5000	5.0000	.0000	69.632	47.183	7.317	297.4
3	10.5000	5.0000	.0000	72.046	49.451	13.219	449.5
3	10.5000	5.0000	.0000	115.518	49.750	34.750	449.5
3	10.5000	5.0000	.0000	88.435	46.972	18.146	449.5
3	10.5000	5.0000	.0000	91.797	46.242	25.077	643.4
3	10.5000	5.0000	.0000	75.906	46.818	14.888	643.4
3	10.5000	5.0000	.0000	124.875	48.218	51.262	643.4
1	10.5000	4.5000	.0000	80.364	38.650	12.526	646.4
1	10.5000	4.5000	.0000	151.242	38.374	43.023	646.4
1	10.5000	4.5000	.0000	69.892	39.010	9.427	646.4
1	10.5000	4.5000	.0000	111.854	39.708	22.905	646.4
1	10.5000	4.5000	.0000	59.364	44.837	3.673	646.4
1	10.5000	4.5000	.0000	95.048	37.776	17.957	646.4
1	10.5000	4.5000	.0000	162.340	38.052	49.777	646.4
1	10.5000	4.5000	.0000	51.181	39.754	4.800	646.4
1	10.5000	4.5000	.0000	120.312	38.834	27.044	646.4
1	10.5000	4.5000	.0000	74.095	40.167	9.678	646.4
1	10.5000	4.5000	.0000	136.511	38.512	35.025	646.4
1	10.5000	4.5000	.0000	58.400	35.793	8.640	646.4
1	10.5000	4.5000	.0000	126.508	38.604	30.805	646.4
1	10.5000	4.5000	.0000	100.216	39.662	18.408	646.4
1	10.5000	4.5000	.0000	88.440	44.198	11.289	646.4
1	10.5000	7.0000	.0000	80.456	41.574	23.568	646.4
1	10.5000	7.0000	.0000	140.787	38.282	89.389	646.4
1	10.5000	7.0000	.0000	64.406	37.975	21.275	646.4
1	10.5000	7.0000	.0000	101.575	38.972	47.153	646.4
1	10.5000	7.0000	.0000	171.621	40.197	126.974	646.4
1	10.5000	7.0000	.0000	124.271	40.351	70.091	646.4

1	10.5000	7.0000	.0000	159.296	40.886	109.925	646.4
1	10.5000	7.0000	.0000	57.163	36.900	20.128	646.4
1	10.5000	7.0000	.0000	88.766	38.589	38.186	646.4
1	10.5000	7.0000	.0000	162.204	39.432	118.182	646.4
1	10.5000	7.0000	.0000	73.064	41.497	22.657	646.4
1	10.5000	7.0000	.0000	109.764	37.361	59.744	646.4
1	10.5000	7.0000	.0000	135.127	42.032	79.877	646.4
1	10.5000	7.0000	.0000	96.989	41.879	40.702	646.4
1	10.5000	9.0000	.0000	140.445	44.776	165.541	646.4
1	10.5000	9.0000	.0000	70.424	43.710	33.545	646.4
1	10.5000	9.0000	.0000	93.102	42.719	73.504	646.4
2	10.5000	4.5000	.3083	116.409	38.435	39.498	646.4
2	10.5000	4.5000	.3083	154.612	36.823	76.730	646.4
2	10.5000	4.5000	.3083	84.956	37.361	22.248	646.4
2	10.5000	4.5000	.3083	95.695	40.198	25.075	646.4
2	10.5000	4.5000	.3083	142.922	37.591	59.922	646.4
2	10.5000	4.5000	.3083	103.967	36.823	33.188	646.4
2	10.5000	4.5000	.3083	160.815	37.438	75.691	646.4
2	10.5000	4.5000	.3083	131.104	37.438	50.100	646.4
2	10.5000	4.5000	.3083	56.263	37.745	10.882	646.4
2	10.5000	4.5000	.3083	75.749	37.207	18.844	646.4
2	10.5000	4.5000	.3083	64.443	38.282	12.210	646.4
2	10.5000	4.5000	.3083	127.687	38.819	45.353	646.4
2	10.5000	7.0000	.5429	99.463	40.963	28.333	646.4
2	10.5000	7.0000	.5429	137.236	43.558	46.725	646.4
2	10.5000	7.0000	.5429	152.162	43.558	55.375	646.4
2	10.5000	7.0000	.5429	163.959	45.765	65.392	646.4
2	10.5000	7.0000	.5429	69.116	39.126	19.784	646.4
2	10.5000	7.0000	.5429	120.417	40.274	41.079	646.4
2	10.5000	7.0000	.5429	82.663	38.742	21.191	646.4
2	10.5000	7.0000	.5429	77.949	42.337	19.034	646.4
2	10.5000	7.0000	.5429	98.926	43.329	25.332	646.4
2	10.5000	7.0000	.5429	170.815	39.662	79.919	646.4
2	10.5000	7.0000	.5429	66.560	41.268	17.374	646.4
2	10.5000	7.0000	.5429	120.523	43.863	37.614	646.4
2	10.5000	7.0000	.5429	89.635	38.665	30.208	646.4
2	10.5000	7.0000	.5429	64.889	36.054	24.809	646.4
2	10.5000	7.0000	.3143	67.863	43.405	24.749	646.4
2	10.5000	7.0000	.3143	85.533	45.765	32.892	646.4
2	10.5000	7.0000	.3143	96.742	47.663	37.771	646.4
2	10.5000	7.0000	.3143	67.799	46.676	19.586	646.4
2	10.5000	7.0000	.3143	123.242	43.329	68.504	646.4
2	10.5000	7.0000	.3143	148.212	45.613	98.694	646.4

2	10.5000	7.0000	.3143	137.488	47.739	81.999	646.4
2	10.5000	7.0000	.3143	163.352	48.799	116.331	646.4
2	10.5000	7.0000	.3143	176.632	47.511	141.981	646.4
2	10.5000	7.0000	.3143	184.377	46.980	157.555	646.4
2	10.5000	7.0000	.3143	104.960	45.917	49.638	646.4
2	10.5000	7.0000	.3143	116.500	48.724	56.751	646.4
2	10.5000	7.0000	.3143	79.910	48.799	23.810	646.4
2	10.5000	4.5000	.7333	146.274	39.355	85.741	646.4
2	10.5000	4.5000	.7333	64.236	35.053	24.048	646.4
2	10.5000	4.5000	.7333	57.774	36.131	19.609	646.4
2	10.5000	4.5000	.7333	129.047	39.891	62.138	646.4
2	10.5000	4.5000	.7333	183.072	40.351	120.848	646.4
2	10.5000	4.5000	.7333	102.177	43.710	33.618	646.4
2	10.5000	4.5000	.7333	163.236	38.435	99.714	646.4
2	10.5000	4.5000	.7333	104.410	35.285	48.754	646.4
2	10.5000	4.5000	.7333	117.888	36.439	64.014	646.4
2	10.5000	4.5000	.7333	76.394	38.895	24.704	646.4
2	10.5000	4.5000	.7333	89.387	41.498	28.541	646.4
2	10.5000	4.5000	.7333	133.335	38.972	67.568	646.4
2	10.5000	4.5000	.7333	155.109	41.115	85.558	646.4
2	10.5000	4.5000	.7333	181.253	45.613	107.632	646.4
3	10.5000	4.0000	.0000	83.537	38.627	17.274	646.4
3	10.5000	4.0000	.0000	148.435	39.585	52.109	646.4
3	10.5000	4.0000	.0000	119.259	38.857	35.904	646.4
3	10.5000	4.0000	.0000	55.948	38.013	6.783	646.4
3	10.5000	4.0000	.0000	133.624	39.010	43.569	646.4
3	10.5000	4.0000	.0000	172.706	40.044	68.628	646.4
3	10.5000	4.0000	.0000	65.830	38.313	10.641	646.4
3	10.5000	4.0000	.0000	106.937	38.090	29.329	646.4
3	10.5000	4.0000	.0000	183.893	38.129	78.614	646.4
3	10.5000	4.0000	.0000	158.118	38.512	60.790	646.4
3	10.5000	4.0000	.0000	73.830	39.853	13.143	646.4
3	10.5000	4.0000	.0000	124.265	37.438	39.402	646.4
3	10.5000	4.0000	.0000	177.293	37.898	74.505	646.4
3	10.5000	4.0000	.0000	96.191	38.052	22.987	646.4
3	10.5000	5.0000	.0000	100.197	41.077	39.589	646.4
3	10.5000	5.0000	.0000	60.008	40.962	11.603	646.4
3	10.5000	5.0000	.0000	143.778	42.490	66.405	646.4
3	10.5000	5.0000	.0000	164.696	36.631	98.182	646.4
3	10.5000	5.0000	.0000	71.737	37.630	19.376	646.4
3	10.5000	5.0000	.0000	69.370	42.260	11.520	646.4
3	10.5000	5.0000	.0000	117.041	37.860	49.749	646.4
3	10.5000	5.0000	.0000	130.720	37.092	62.004	646.4
3	10.5000	5.0000	.0000	84.628	36.477	28.411	646.4
3	10.5000	5.0000	.0000	111.640	38.820	43.025	646.4

3	10.5000	5.0000	.0000	151.818	37.630	81.319	646.4
3	10.5000	5.0000	.0000	79.029	38.205	23.351	646.4
3	10.5000	5.0000	.0000	58.429	41.134	11.055	646.4
3	10.5000	6.4000	.0000	138.066	37.745	96.824	646.4
3	10.5000	6.4000	.0000	113.021	36.247	67.327	646.4
3	10.5000	6.4000	.0000	66.309	37.092	21.642	646.4
3	10.5000	6.4000	.0000	77.180	38.167	29.026	646.4
3	10.5000	6.4000	.0000	150.782	38.550	113.390	646.4
3	10.5000	6.4000	.0000	171.948	37.668	143.439	646.4
3	10.5000	6.4000	.0000	89.418	39.128	39.027	646.4
3	10.5000	6.4000	.0000	130.244	38.244	82.742	646.4
3	10.5000	6.4000	.0000	96.065	37.015	47.940	646.4
3	10.5000	6.4000	.0000	180.199	38.589	155.999	646.4
3	10.5000	6.4000	.0000	162.411	39.547	126.942	646.4
3	10.5000	6.4000	.0000	62.741	38.857	15.391	646.4
3	10.5000	6.4000	.0000	121.076	36.823	74.285	646.4
3	10.5000	6.4000	.0000	81.815	37.591	33.772	646.4

BIBLIOGRAPHY

1. Ratzel, A. C., Hickox, C. E., and Gartling, D. K., Techniques for Reducing Conduction and Natural Convection Heat Losses in Annular Receiver Geometries, Transactions of the ASME, Journal of Heat Transfer, Vol. 101, pp. 108-113, 1979.

2. Ratzel, A. C., and Simpson, C. E., Heat Loss Reduction Techniques for Annular Solar Receiver Designs, Sandia Laboratories Report SAND 78-1769, Sandia Laboratories, Albuquerque, NM, 1978.

3. Buchberg, H., Catton, I., and Edwards, D. K., Natural Convection in Enclosed Spaces--A Review of Application to Solar Energy Collection, Transactions of the ASME, Journal of Heat Transfer, Vol. 98, pp. 182-188, 1976.

4. Raithby, G. D., and Hollands, K. G. T., A General Method of Obtaining Approximate Solutions to Laminar and Turbulent Free Convection Problems, Advances in Heat Transfer, Vol. 11, pp. 265-315, 1975.

5. Bird, R. B., Stewart, W. E., and Lightfoot, E. N., Transport Phenomena, John Wiley and Sons, Inc., New York, 1960.

6. Holman, J. P., Heat Transfer, Fourth Edition, McGraw-Hill Book Company, New York, 1976.

7. Elenbaas, W., The Dissipation of Heat by Free Convection from Vertical and Horizontal Cylinders, Journal of Applied Physics, Vol. 19, pp. 1148-1154, 1948.

8. Gebhart, B., Heat Transfer, Second Edition, McGraw-Hill Book Company, New York, 1971.

9. Lienhard, J. H., On the Commonality of Equations for Natural Convection from Immersed Bodies, International Journal of Heat and Mass Transfer, Vol. 16, pp. 2121-2123, 1973.

10. Saunders, O. A., The Effect of Pressure Upon Natural Convection in Air, Proceedings of the Royal Society of London, Vol. 157A, pp. 278-291, 1936.

11. Kyte, J. R., Madden, A. J., and Piret, E. L., Natural Convection Heat Transfer at Reduced Pressure, Chemical Engineering Progress, pp. 653-662, 1953.

12. Gryzagoridis, J., Natural Convection From a Vertical Flat Plate in the Low Grashof Number Range, International Journal of Heat and Mass Transfer, Vol. 14, pp. 162-165, 1971.

13. Suriano, F. J., and Yang, K. T., Laminar Free Convection About Vertical and Horizontal Plates at Small and Moderate Grashof Numbers, International Journal of Heat and Mass Transfer, Vol. 11, pp. 473-490, 1968.

14. Chiang, T, Ossin, A., and Tien, C. L., Laminar Free Convection from a Sphere, Transactions of the ASME, Journal of Heat Transfer, Vol. 86, pp. 537-542, 1964.

15. Lin, F. N., and Chao, B. T., Laminar Free Convection Over Two-Dimensional and Axisymmetric Bodies of Arbitrary Contour, Transactions of the ASME, Journal of Heat Transfer, Vol. 96, pp. 435-442, 1974.

16. Saville, D. A., and Churchill, S. W., Laminar Free Convection on Boundary Layers Near Horizontal Cylinders and Vertical Axisymmetric Bodies, Journal of Fluid Mechanics, Vol. 29, pp. 391-399, 1967.

17. Sparrow, E. M., and Gregg, J. L., Laminar Free Convection Heat Transfer From the Outer Surface of a Vertical Circular Cylinder, Transactions of the ASME, pp. 1823-1829, 1956.

18. Minkowycz, W. J., and Sparrow, E. M., Local Nonsimilar Solutions for Natural Convection on a Vertical Cylinder, Transactions of the ASME, Journal of Heat Transfer, Vol. 96, pp. 178-183, 1974.

19. Churchill, S. W., and Churchill, R. U., A Comprehensive Correlating Equation for Heat and Component Transfer by Free Convection, American Institute of Chemical Engineers, Journal, Vol. 21, pp. 604-606, 1975.

20. Elenbaas, W., Heat Dissipation of Parallel Plates by Free Convection, Physics, Vol. 9, pp. 1-28, 1942.

21. Batchelor, G. K., Heat Transfer by Free Convection Across a Closed Cavity Between Vertical Boundaries at Different Temperatures, Quarterly of Applied Mathematics, Vol. 12, pp. 209-233, 1954.

22. Newell, M. E., and Schmidt, F. W., Heat Transfer by Laminar Natural Convection Within Rectangular Enclosures, Transactions of the ASME, Journal of Heat Transfer, Vol. 92, pp. 159-168, 1970.

23. Randall, K. R., Mitchell, J. W., and El-Wakil, M. M., Natural Convection Heat Transfer Characteristics of Flat Plate Enclosures, Transactions of the ASME, Journal of Heat Transfer, Vol. 101, pp. 120-125, 1979.

24. Flack, R. D., Konopnicki, T. T., and Rooke, J. H., The Measurement of Natural Convective Heat Transfer in Triangular Enclosures, Transactions of the ASME, Journal of Heat Transfer, Vol. 101, pp. 648-654, 1979.

25. Scanlan, J. A., Bishop, E. H., and Powe, R. E., Natural Convection Heat Transfer Between Concentric Spheres, International Journal of Heat and Mass Transfer, Vol. 13, pp. 1857-1872, 1970.

26. Kuehn, T. H., and Goldstein, R. J., an Experimental and Theoretical Study of Natural Convection in the Annulus Between Horizontal Concentric Cylinders, Journal of Fluid Mechanics, Vol. 74, pp. 695-719, 1976.

27. Kuehn, T. H., and Goldstein, R. J., Correlating Equations for Natural Convection Heat Transfer Between Horizontal Circular Cylinders, International Journal of Heat and Mass Transfer, Vol. 19, pp. 1127-1134, 1976.

28. Kuehn, T. H., and Goldstein, R. J., An Experimental Study of Natural Convection Heat Transfer in Concentric and Eccentric Horizontal Cylindrical Annuli, Transactions of the ASME, Journal of Heat Transfer, Vol. 100, pp. 635-640, 1978.

29. Mack, L. R., and Hardee, H. C., Natural Convection Between Concentric Spheres at Low Rayleigh Numbers, International Journal of Heat Transfer, Vol. 11, pp. 387-396, 1968.

30. Mack, L. R., and Bishop, E. H., Natural Convection Between Horizontal Concentric Cylinders for Low Rayleigh Numbers, Quarterly Journal of Mechanics and Applied Mathematics, Vol. 31, pp. 223-241, 1968.

31. Koshmarov, Y. A., and Ivanov, A. Y., Experimental Study of Heat Transfer Through a Rarefied Gas Between Coaxial Cylinders, Heat Transfer--Soviet Research, Vol. 5, pp. 29-36, 1973.

32. Marker, G. P., and Leal, L. G., Natural Convection in a Shallow Annular Cavity, International Journal of Heat and Mass Transfer, Vol. 23, pp. 677-686, 1980.

33. Warrington, R. O., Natural Convection Heat Transfer Between Bodies and Their Enclosures, Ph.D. Dissertation, Montana State University, 1975.

34. Kennard, E. H., Kinetic Theory of Gases, McGraw-Hill, New York, 1938.

35. Dushman, S., Scientific Foundations of Vacuum Technique, Second Edition, (J. M. Lafferty, ed.), Wiley, New York, 1962.

36. Guthrie, A., Vacuum Technology, Wiley, New York, 1963.

37. Bishop, E. H., Heat Transfer by Natural Convection Between Isothermal Concentric Spheres, Ph.D. Dissertation, University of Texas, Austin, 1964.

38. Rohsenow, W. M., and Choi, H. Y., Heat, Mass, and Momentum Transfer, Prentice-Hall, Englewood Cliffs, New Jersey, 1961.

39. Bandrowski, J., and Rybski, W., Free Convection Mass Transfer from Horizontal Plates, International Journal of Heat and Mass Transfer, Vol. 19, pp. 827-838, 1976.

40. Warrington, R. O., personal conversations.

41. McCoy, C. T., Powe, R. E., Bishop, E. H., Weber, N., and Scanlan, J. A., Free Convection Between a Vertical Cylinder and a Spherical Enclosure, Proceedings of the Fifth International Heat Transfer Conference, Tokyo, 1974.

42. Bishop, E. H., Mack, L. R., and Scanlan, J. A., Heat Transfer by Natural Convection Between Concentric Spheres, International Journal of Heat and Mass Transfer, Vol. 9, pp. 649-661, 1966.

43. Itoh, M., Fujita, T., Nishiwaki, N., and Hirata, M., A New Method of Correlating Heat Transfer Coefficients for Natural Convection in Horizontal Cylindrical Annuli, International Journal of Heat and Mass Transfer, Vol. 13, pp. 1364-1368, 1970.

MONTANA STATE UNIVERSITY LIBRARIES
3 1762 10013126 5

[redacted]

N378
B8145
cop.2

Brown, Peter K
Natural convection heat transfer within enclosures at reduced pressures

DATE	ISSUED TO
FEB 2	ARLEN ROESNER (5) 7-5019 THO A JULIA MARTIN
	Dale Wallace 631 E JAMES #4 G-7537
	D_W
new due date 5-9-	
	[redacted]
2 WEEKS	INTERI
	9-2

[redacted]

N378
B8145
cop 2